


2015

Cellular level studies and coil system design for transcranial magnetic stimulation

Yiwen Meng
Iowa State University

Follow this and additional works at: <https://lib.dr.iastate.edu/etd>

 Part of the [Biomedical Commons](#), and the [Electrical and Electronics Commons](#)

Recommended Citation

Meng, Yiwen, "Cellular level studies and coil system design for transcranial magnetic stimulation" (2015). *Graduate Theses and Dissertations*. 14511.
<https://lib.dr.iastate.edu/etd/14511>

This Thesis is brought to you for free and open access by the Iowa State University Capstones, Theses and Dissertations at Iowa State University Digital Repository. It has been accepted for inclusion in Graduate Theses and Dissertations by an authorized administrator of Iowa State University Digital Repository. For more information, please contact digirep@iastate.edu.

Cellular level studies and coil system design for transcranial magnetic stimulation

by

Yiwen Meng

A thesis submitted to the graduate faculty
in partial fulfillment of the requirements for the degree of

MASTER OF SCIENCE

Major: Electrical Engineering

Program of Study Committee:
David.C.Jiles, Co-Major Professor
Ravi.M.Hadimani, Co-Major Professor
Long Que

Iowa State University

Ames, Iowa

2015

Copyright © Yiwen Meng, 2015. All rights reserved.

DEDICATION

I would like to dedicate this thesis to my mother Li and my father Yulin for their unconditional and tremendous love and support for me to overcome any difficulty I met.

TABLE OF CONTENTS

	Page
LIST OF FIGURES	v
LIST OF TABLES	viii
ACKNOWLEDGEMENT	ix
ABSTRACT	x
CHAPTER 1. GENERAL INTRODUCTION	1
Transcranial Magnetic Stimulation.....	1
Research Motivation.....	2
Thesis Organization.....	3
References.....	4
CHAPTER 2. DIFFERENTIAL EFFECT OF MAGNETIC FIELD	
ORIENTATION ON THE PROLIFERATION RATE OF DOPAMINERGIC	
NEURONS DURING TRANSCRANIAL MAGNETIC STIMULATION	5
Abstract.....	5
Introduction.....	6
Experimental Procedures.....	7
Results.....	15
Discussions.....	19
Conclusions.....	21
References.....	22

CHAPTER 3. THERMAL AND MECHANICAL ANALYSIS OF VARIABLE	
TMS COIL SYSTEM.....	24
Abstract.....	24
Introduction.....	24
Magnetic (Lorentz) Force Response.....	25
Thermal Analysis.....	27
GUI system.....	28
Conclusion.....	28
References.....	29
CHAPTER 4.GENERAL CONCLUSIONS.....	31
General Discussion.....	31
Recommendation for Future Research.....	32
References.....	33
APPENDIX A. SIMULATION RESULTS OF ELECTROMAGNETIC FIELD	
FOR VARIABLE TMS COIL SYSTEM.....	33
References.....	35
APPENDIX B. LIST OF PUBLICATIONS AND REPRINTS OF	
PUBLICATIONS DERIVED FROM THE WORK PERFORMED FOR THIS	
THESIS	36

LIST OF FIGURES

	Page
Figure.1 The illustration of TMS treatment on human brain.....	1
Figure.2 Illustration of research areas on TMS	2
Figure.3 The axial component of magnetic field intensity along the diameter of a Magtism® Standard 70 mm double coil at coil surface. The red line is simulation result from SEMCAD X and the black line is measured result using gauss meter. The intensity of Magstim Rapid ² stimulator was 100%.....	8
Figure.4 The axial component of magnetic field intensity along the diameter of a Magtism® Standard 70 mm double coil at height of 5mm above coil surface. The red line is simulation result from SEMCAD X and the black line is measured result using gauss meter. The intensity of Magstim Rapid ² stimulator was 100%	8
Figure.5 Distribution of magnetic field intensity of double coil (2D top view).....	9
Figure 6 Orientation of magnetic flux lines generated by double coil, cross representing upward and dot representing downward field. The red arrows show the direction of supplied current with a peak magnitude of 5000 A. The two blue polygons represent the two flasks.....	9
Figure 7 Distribution of induced current on the coil plane at the first half of period of supplied current (2D top view).....	9
Figure 8 Distribution of induced current on the coil plane at the second half of period of supplied current (2D top view).....	9
Figure 9 Arrangement of the 30-minute TMS treatment delivered to two T-75 flasks. The directions of the two oppositely oriented magnetic fields were labeled on the double coil. Field orientation was upward on the left coil and downward on the right coil, as shown in the inset figure. We used two clamps to fix the coil in the cell culture cabinet and a layer of bubble wrap separated both flasks from the coils to maintain a thermal barrier.....	12
Figure 10 Cell densities in the TMS experiment, derived using the Trypan blue cell counting method with an initial seeding density of 1 million cells/flask. Counting time is indicated in Table. I.....	16
Figure 11 Cell densities in the TMS experiment, derived using the Trypan blue cell counting method with an initial seeding density of 0.5 million cells/flask. Counting time is indicated in Table. I.....	16

- Figure 12 Cell densities in the TMS experiment, derived using the Trypan blue cell counting method for an initial seeding density of 0.5 million cells/flask. Culture times were Day 0.5, Day 1, Day 1.5, Day 2 and Day 2.5. The corresponding Counting times were Day 1.5, Day 2, Day 2.5, Day 3 and Day 3.5, respectively.....17
- Figure 13 Cell proliferation after TMS treatment of plates with an initial seeding density of 20k/well. We used the CyQuant cell viability assay to count cells. On day 3, the number of cells in the “Field up” group was $22.06 \pm 4.14\%$ (mean \pm STD as a percentage of the initial seeding density, * $p < 0.05$) higher than in the Environmental group, whereas cell numbers in the “Field down” group were $28.77 \pm 1.00\%$ (** $p < 0.01$) lower than in the Environmental group.....18
- Figure 14 Cell proliferation after TMS treatment of plates with an initial seeding density of 50k/well. We used the CyQuant cell viability assay to count cells. On day 3, the number of cells in the “Field up” group was $15.49 \pm 7.26\%$ (mean \pm STD as a percentage of the initial seeding density, * $p < 0.05$) higher than in the Environmental group, whereas cell numbers in the “Field down” group were $9.94 \pm 2.47\%$ (* $p < 0.05$) lower than in the Environmental group.....18
- Figure 15 Cell proliferation after TMS treatment of plates with an initial seeding density of 80k/well. We used the CyQuant cell viability assay to count cells. On day 3, the number of cells in the “Field up” group was $15.57 \pm 5.17\%$ (mean \pm STD as a percentage of the initial seeding density, * $p < 0.05$) higher than in the Environmental group, whereas cell numbers in the “Field down” group were $11.62 \pm 1.55\%$ (* $p < 0.05$) lower than in the Environmental group.....18
- Figure 16 Cell proliferation after TMS treatment of plates with an initial seeding density of 100k/well. We used the CyQuant cell viability assay to count cells. On day 3, the number of cells in the “Field up” group was $14.69 \pm 5.74\%$ (mean \pm STD as a percentage of the initial seeding density, $p > 0.05$) higher than in the Environmental group, whereas cell numbers in the “Field down” group were the same ($0 \pm 4.50\%$, $p > 0.05$) as those in the Environmental group.....17
- Figure 17 Cell proliferation after TMS treatment of plates with an initial seeding density of 15k/well. We used the MTS cell viability assay to count cells, reported here as a percentage of control group1 (Incubator).....19
- Figure 18 Cell proliferation after TMS treatment of plates with an initial seeding density of 20k/well. We used the MTS cell viability assay to count cells, reported here as a percentage of control group1 (Incubator).....19
- Figure 19 The result of force analysis between the two coils with larger coil rotated at $+30^\circ$. In (a) and (b), the distance between the centers of two coils is 5 cm, while (a) is the top view, (b) is the side view. In (c) and (d), the distance between the centers of two coils is 15 cm, while (c) is the top view, (d) is the side view.....26

Figure 20 The result of thermal analysis of two coils with larger coil rotated at $+30^\circ$. In (a) and (b), the distance between the centers of two coils is 5 cm, while (a) is the top view, (b) is the side view. In (c) and (d), the distance between the centers of two coils is 15 cm, while (c) is the top view, (d) is the side view.....	26
Figure 21 The graphic user interface (GUI).....	28
Figure 22 Magnetic field (a and c) and electric field (b and d) generated in the anatomically realistic human head model for different vertical positions of the large coil. In figures a and b, the distance between two coils is 5 cm. In figures c and d, the distance between two coils is 15 cm.....	35
Figure 23 Magnetic field (a and c) and electric field (b and d) generated in the anatomically realistic human head model for different rotational angles of the large coil. In figures a and b, the coil is rotated $+30$ degrees. In figures c and d, the coil is rotated -30 degrees.....	35

LIST OF TABLES

	Page
Table 1 Design of the TMS experiment with Trypan blue cell counting method for cell densities of 1 and 0.5 million cells /flask.	13
Table 2 Design of the TMS experiment with CyQuant cell viability assay cell counting method for cell densities of 100k, 80k, 50k and 20k per well.....	13
Table 3 Design of the TMS experiment with MTS cell viability assay cell counting method for cell densities of 15k and 20k per well.....	14
Table 4 Values of Dielectric Properties at 2.5 kHz.....	34

ACKNOWLEDGEMENTS

I would like to thank my major professor Dr.Jiles and Dr. Hadimani and my committee member Dr. Que for their guidance and support throughout the course of this research.

In addition, I would also like to thank my friends, colleagues, the department faculty and staff for making my time at Iowa State University a wonderful experience. I want to also offer my appreciation to our collaborators in Dr. Kanthasamy's Group in College of Veterinary Medicine for their genuine help in cellular studies.

ABSTRACT

Transcranial Magnetic Stimulation is a novel non-invasive neuromodulation technique to treat human brain disorders such as depression, Parkinson's disease and PTSD. It uses pulsed currents in the coils to generate time varying magnetic field which induce eddy currents in the conductive tissues of the human brain. Recently, there have been many research publications in the field of TMS, specifically on coil designs, clinical trials and some in-vivo animal studies.

Even though FDA has approved TMS technique to treat depression, the basic mechanism or how the neural tissue reacts to TMS is still not well understood. Therefore, conducting in-vitro study on TMS will enable researchers to understand how TMS has influence on neural cells and neural tissue growth rate, morphology, axon length and other factors. In this work, I have conducted experiments on effect of TMS on N27 dopaminergic neural cells, an immortal cell line of rat, to investigate the effect on cell's growth rate. Results will enable neuroscientists to understand the mechanism of TMS on neural cells.

As a part of TMS project, I have also worked on the development of a TMS helmet design. Due to the limitation of patient's head size and rapid decay rate of magnetic field away from coil surface, designing an efficient and compact coil system is needed to treat deep brain regions. We have developed a variable coil system with combination of fixed single coil on top and variable Halo coil to realize deep brain stimulation with automatic control system and graphic user interface (GUI). In the meantime, I also conducted thermal and mechanical analysis of new coil configuration to investigate heating effect and electromagnetic force on the whole coil system. This system can be used by researchers or

clinicians with relative ease, maintaining the accuracy of coil position relative to the patients head.

CHAPTER 1.GENERAL INTRODUCTION

Transcranial Magnetic Stimulation (TMS)

Transcranial Magnetic Stimulation (TMS) is a non-invasive neuromodulation technique which has potential to treat various neurological disorders such as major depressive disorder, Parkinson's disease, Post-traumatic stress disorder (PTSD) and migraine non-invasively and safely. It uses short pulses of time varying magnetic field to induce an electric field in the conductive tissues of the brain, hence, modulating the synaptic transmission of neurons. This neuromodulation technique can be used to excite or inhibit the firing rate of neurons by influencing the ion activities inside and outside of neuron's plasma membrane [1-5].

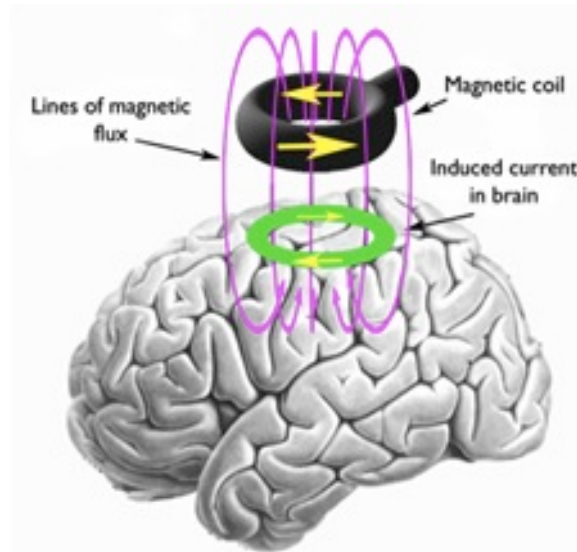


Fig.1 The illustration of TMS treatment on human brain (from Laboratory for cognition and neural stimulation in school of medicine at University of Pennsylvania)

Fig.1 illustrates the basic mechanism of TMS and how it affects brain behavior of human. TMS uses different types of coils such as single coil, double coil, Halo coil and Helmholtz coil to generate different types of magnetic field in the human brain. In clinical trials, physicians put

certain type of coil according to the specific region of human brain like hippocampus and motor cortex to treat specific brain disorders [5].

Research Motivation

Since the US Food and Drug Administration (FDA) approved TMS as a treatment for depression in 2008, there has been an increasing research interest on TMS. As shown in Fig.2, the major fields are computer modeling and coil design, in-vitro and in-vivo studies and clinical trials [6-7]. More importantly, understanding the mechanism of TMS on brain or how TMS affects individual neurons or neural tissues would bring a big breakthrough to the current theory.

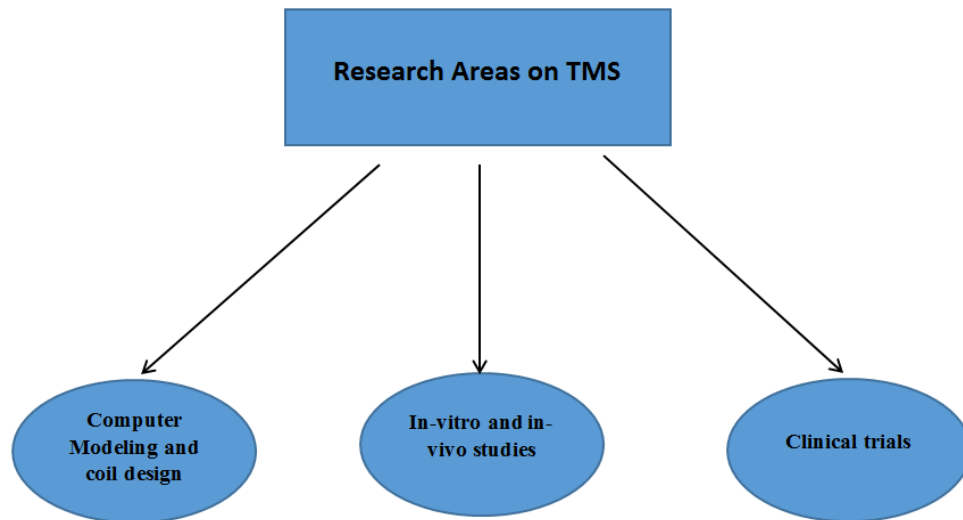


Fig. 2 Illustration of research areas on TMS

Therefore, doing in-vitro study on TMS is a good approach to investigate effect of TMS on several parameters like growth rate, soma size of individual neurons or neural networks. These kinds of work would be addressed into the study on growth rate, morphology and protein analysis of neurons. The motor symptoms of Parkinson's disease result from the death of dopamine generating cells in the midbrain region, substantial nigra. 1RB3AN27 cell line is the immortalized dopamine neural cells from rat brain. This immortalized cell line has been carefully

characterized in studies of dopamine biosynthesis, neurotoxicity and used as a dopaminergic neuron model for in vitro and in vivo studies. Therefore, there have been numerous efforts to understand the basic mechanism of the degenerative process of dopaminergic neurons and to realize neural genesis in substantial nigra to cure Parkinson's disease [8].

Besides, another aspect of research on TMS is designing efficient, compact coils or a coil system to treat different regions of the human brain especially the deep-lying regions. Thus, overcoming the fast decay rate of the magnetic field to induce enough electromagnetic fields in deep brain regions is one big challenge right now. Meanwhile, building a compact or even an automatic TMS coil system will make it easier for doctors to conduct TMS treatment in clinical trials.

Thesis Organization

Chapter 2 and Chapter 3 describe two parts of my work on TMS, focusing on in-vitro and coil design of TMS, respectively. Chapter 2 mainly shows the effect on different orientation of magnetic field on the proliferation rate of dopaminergic neurons with three different cell counting methods. It also gives a literature review of the beneficial effect of static and time varying electromagnetic field with different frequency ranges. Chapter 3 mainly describes work on computer modeling of thermal and mechanical analysis of variable TMS coil system and an illustration of graphic user interface (GUI) of the coil system.

Chapter 4 summarizes all of work in this thesis and some recommendations for future work on TMS like morphology study and protein analysis of neurons to understand the mechanism of TMS. References can be found at the end of each chapter. Appendix A lists all of my journal and conference publications during my master's degree. Appendix B shows the results of computer modeling of electromagnetic field for the variable TMS coil system.

References

- [1] Barker AT, Jalinous R, Freeston IL. NON-INVASIVE MAGNETIC STIMULATION OF HUMAN MOTOR CORTEX. *Lancet* 1985;325:1106–7. doi:10.1016/S0140-6736(85)92413-4.
- [2] George MS, Lisanby SH, Sackeim HA. Transcranial Magnetic Stimulation. *Arch Gen Psychiatry* 1999;56:300. doi:10.1001/archpsyc.56.4.300.
- [3] Vonloh M, Chen R, Kluger B. Safety of transcranial magnetic stimulation in Parkinson's disease: a review of the literature. *Parkinsonism Relat Disord* 2013;19:573–85. doi:10.1016/j.parkreldis.2013.01.007.
- [4] Rosenberg PB. Repetitive Transcranial Magnetic Stimulation Treatment of Comorbid Posttraumatic Stress Disorder and Major Depression. *J Neuropsychiatr* 2002;14:270–6. doi:10.1176/appi.neuropsych.14.3.270.
- [5] Dodick DW, Schembri CT, Helmuth M, Aurora SK. Transcranial magnetic stimulation for migraine: a safety review. *Headache* 2010;50:1153–63. doi:10.1111/j.1526-4610.2010.01697.x.
- [6] Crowther LJ, Hadimani RL, Jiles DC. A numerical dosimetry study for pediatric transcranial magnetic stimulation. 2013 6th Int. IEEE/EMBS Conf. Neural Eng., IEEE; 2013, p. 239–42. doi:10.1109/NER.2013.6695916.
- [7] Wassermann EM, Zimmermann T. Transcranial magnetic brain stimulation: therapeutic promises and scientific gaps. *Pharmacol Ther* 2012;133:98–107. doi:10.1016/j.pharmthera.2011.09.003.
- [8] M. Carvour, C. Song, S. Kaul, V. Anantharam, A. Kanthasamy, and A. Kanthasamy, "Chronic low-dose oxidative stress induces caspase-3-dependent PKCdelta proteolytic activation and apoptosis in a cell culture model of dopaminergic neurodegeneration.," *Ann. N. Y. Acad. Sci.*, vol. 1139, pp. 197–205, 2008.

CHAPTER 2. DIFFERENTIAL EFFECT OF MAGNETIC FIELD ORIENTATION ON THE PROLIFERATION RATE OF DOPAMINERGIC NEURONS DURING TRANSCRANIAL MAGNETIC STIMULATION

Modified from a paper submitted to *Neuroscience of Elsevier*

Y. Meng¹, R. L. Hadimani¹, L. J. Crowther¹, V. Anantharam², Gary Zenitsky², A. Kanthasamy² and D. C. Jiles¹

¹*Dept. of Electrical and Computer Engineering, Iowa State University, Ames, IA 50011 USA*

²*Department of Biomedical Sciences, Iowa State University, Ames, IA 50011, USA*

Abstract

Transcranial magnetic stimulation (TMS) has been used to investigate possible treatments for a variety of neurological disorders. But the effect that magnetic fields have on neurons has not been well documented in the literature. Using a monophasic stimulator, we investigated the effect of different orientation of magnetic field generated by TMS coils on the proliferation rate of N27 neuronal cells cultured in flasks and multi-well plates. Exposing horizontally adherent N27 cells to a magnetic field pointing upward through the neuronal proliferation layer increased the proliferation of cells compared with the control group. On the other hand, proliferation rate decreased in cells exposed to a magnetic field pointing downward through the neuronal growth layer compared with the control group. The results were consistent across different methods of measuring proliferation and cell counting procedures. We confirmed results obtained from the Trypan-blue and automatic cell counting methods with those from the CyQuant and MTS cell viability assays. Our findings could have important implications for the preclinical development of TMS treatments of neurological disorders and represents a new method to control the proliferation rate of neuronal cells.

Key words: TMS; dopaminergic neurons; proliferation rate; orientation of magnetic field

Introduction

Transcranial Magnetic Stimulation is a non-invasive neuromodulation technique that uses time varying short pulses of magnetic field to induce an electric field in the conductive tissues of the brain thus, modulating the synaptic transmission of neurons. This neuromodulation technique can be used to excite or inhibit the firing rate of neurons which can then be used for treatment of various neurological disorders such as major depressive disorder, Parkinson's disease, Post-traumatic stress disorder and migraine [1-5]. Since the US Food and Drug Administration (FDA) approved TMS as a treatment for depression in 2008, there has been less focus on *in vitro* and animal studies in the literature compared to *in vivo* studies in humans [6-8]. The effects of TMS on individual neurons need to be thoroughly understood to fully utilize TMS as a neuromodulation tool for treating neurological disorders especially those originating from subcortical regions of the brain.

Few articles have reported the effect of time-varying magnetic fields, similar to those generated by TMS, on the proliferation rates of neurons. Bonmassar et al. designed micro TMS coils and showed that the direction of magnetic field affects the firing frequency of neurons, but the authors did not report the effect of magnetic field on the proliferation rate [9]. Meanwhile, some articles have reported the effect of static magnetic field on cell's proliferation rate. Authors have used static magnetic fields from 1 to 10 tesla and did not find any significant effect on cell proliferation or on genetic toxicity, regardless of the length of treatment. However, there was a small effect on intracellular Ca^{2+} ion control [10]. Some articles have reported beneficial effects of DC electric field (EF) on neural proliferation and differentiation. The EF gradient affects morphology and phenotype of adult neural stem/progenitor cells (NPCs), which shows the potential of utilizing EF to control migration,

differentiation and alignment of stem cells transplanted to treat nervous system disorders [11]. Extremely low-frequency electromagnetic fields (ELF-EMFs) have been used therapeutically to drive cardiac-specific differentiation in adult human cardiac progenitor cells without any pharmacological or genetic manipulation of cells [12]. As far as we know, no one has published on the effect of TMS magnetic field on the proliferation rate of neurons or on the morphology of cells.

In this paper, we have presented the effect of magnetic field generated by TMS coils on the proliferation of N27 dopaminergic neurons. We have used different cell proliferation and cell counting procedures to confirm that directing a magnetic field downward or upward through the horizontal proliferation plane of adherent cell cultures decreased or increased cell proliferation rates, respectively. It is important to note that the direction of the induced electric current from the time varying TMS fields will be in clockwise or counterclockwise loops when the magnetic field is in up or down direction of the cell culture as shown in Fig. 4. This experimental set up is similar to the TMS treatment on human brain where the induced electric field from the TMS coils will be in clockwise or counterclockwise loops in the cortex.

Experimental procedures

A. Magnetic Field Generated by TMS coils

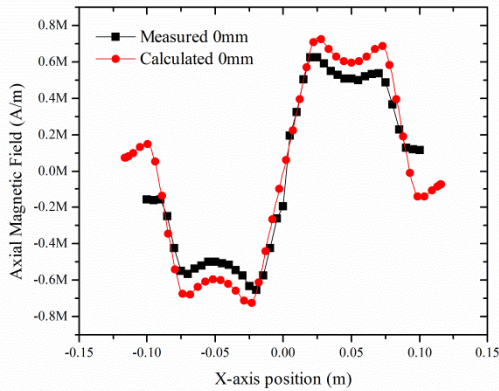


Fig.3 The axial component of magnetic field intensity along the diameter of a Magtism® Standard 70 mm double coil at coil surface. The red line is simulation result from SEMCAD X and the black line is measured result using gauss meter. The intensity of Magstim Rapid² stimulator was 100%.

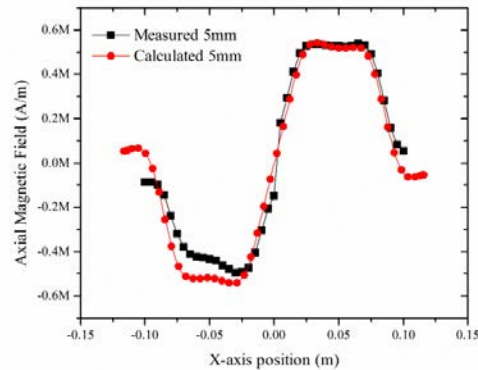


Fig. 4 The axial component of magnetic field intensity along the diameter of a Magtism® Standard 70 mm double coil at height of 5mm above coil surface. The red line is simulation result from SEMCAD X and the black line is measured result using gauss meter. The intensity of Magstim Rapid² stimulator was 100%.

A Magstim Standard 70 mm double coil was used for treating N27 neurons. Magnetic field was measured on the surface of the coil using a gaussmeter and a Hall probe. The field was also calculated using finite element electromagnetic modeling software, SEMCAD X. The measured and calculated axial components of the magnetic field intensities are shown in Fig.3 and Fig.4. Magnetic field is negative in the negative x-axis and positive in the positive x-axis which is shown Fig. 4. It also shows magnetic field values at 5mm above the coil surface where dopaminergic neurons are placed during TMS treatment after considering the thickness of flask and thermal insulation layer. According to these figures, the peak value of measured magnetic field intensity at 5mm above the coil surface is 0.55 MA/m which is reduced by approximately 0.1MA/m. Fig. 5 shows the top view of distribution of magnetic field intensity generated by double coil. Fig.6 shows the different orientations of magnetic field generated by the coil and directions of current in each circle of the double coil. The red

arrows on the left indicate the directions of supplied current (5000 A) in left circle as counterclockwise and clockwise in the right circle. The cross symbols indicate the magnetic flux pointing into the plane and the dot symbols indicate the magnetic flux pointing out of the plane.

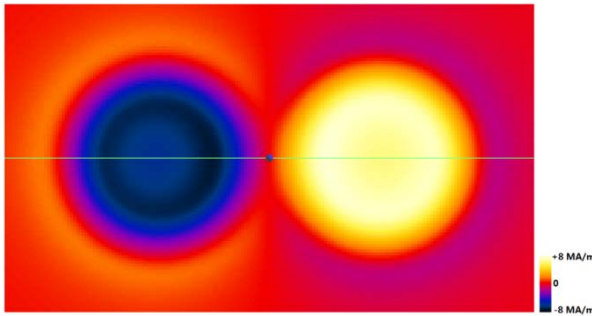


Fig. 5 Distribution of magnetic field intensity of double coil (2D top view).

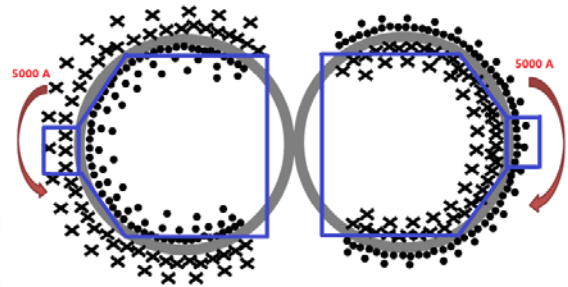


Fig. 6 Orientation of magnetic flux lines generated by double coil, cross representing upward and dot representing downward field. The red arrows show the direction of supplied current with a peak magnitude of 5000 A. The two blue polygons represent the two flasks.

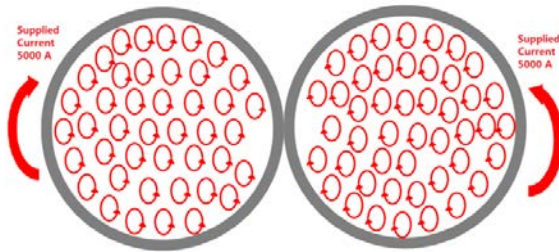


Fig. 7 Distribution of induced current on the coil plane at the first half of period of supplied current (2D top view).

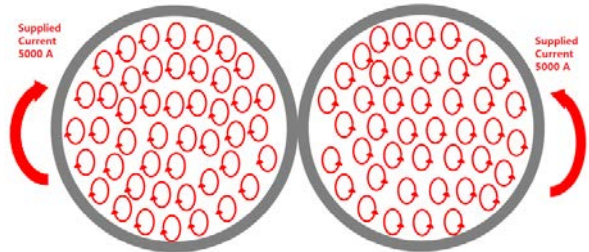


Fig. 8 Distribution of induced current on the coil plane at the second half of period of supplied current (2D top view).

According to Maxwell's equation ($\nabla \times \mathbf{E} = -\frac{\partial \mathbf{B}}{\partial t}$), time-varying magnetic field

will generate an electric field which induces eddy currents in the conducting neurons. The supplied current is a pulse wave which has a frequency of 2.5 kHz and magnitude of 5000 A, so its period is 0.4 ms. The stimulator sends only one pulse with a current amplitude of 5000

A in clockwise and counterclockwise directions in left and right circles of the coil respectively as shown in Fig. 6. Thus, the supplied current in each circular coil will generate a time varying magnetic field changing from 0 to its peak value, during its first half period, which results in the corresponding induced eddy current in both areas shown in Fig. 7 and Fig. 8. According to Lenz's law the induced current in the left circular coil was counterclockwise and it was clockwise in the right circular coil. Similarly, the value of the supplied current in both coils would change from its peak of 5000 A to 0 during the second half period. Thus, the induced eddy currents on the left and right flasks were clockwise and counterclockwise, respectively. Therefore, the difference between the two flasks was the sequence of the direction of the eddy currents.

B. Cell Culture

Immortalized rat mesencephalic 1RB₃AN₂₇ cells (N27) were grown in RPMI-1640 medium supplemented with 10% fetal bovine serum, 1% L-glutamine, 50 units penicillin and 50 µg/ml streptomycin and maintained at 37°C with a humidified atmosphere containing 5% CO₂, as described previously [13,14]. On Day 0, an equal number of N27 cells were seeded into each T-75 flask or 96-well plate. Groups were distinguished by culture time with two control and two TMS groups per time point and four replicate samples (flask or plate) per group. Control 1 was always kept in the incubator and was named Incubator in Table I. Control 2 was kept in the biosafety cabinet during the TMS treatment and was named Environmental in Table I. Table I shows culture time points and counting time points for the different sample locations and magnetic field orientations ("Field up" and "Field down"), which were used in a Trypan blue cytotoxicity assay. Table II shows cell culture samples with their culture time points as well as counting time points used in a CyQuant cell proliferation assay. Table III shows culture samples with their culture and counting time

points for an MTS cell viability assay and cell counting method. We performed a cell count for each sample of cells 24 hours after its TMS treatment to ensure that the cells had enough time to show any effects of TMS on their proliferation.

C. TMS experiment on dopaminergic neurons

We used a monophasic stimulator to treat N27 cell cultures. A set of 6 pulses with 4 seconds waiting time in between them was formed as one train and a waiting time of 10 seconds between each train was introduced, so the pulse repetition rate (TMS treatment frequency) we used is 0.25 Hz. This is a low frequency compared to usual clinical protocol frequency however, in order to obtain 100% power in the coil and avoid rapid heating up of the coil we have used this low frequency. It is not possible to operate at higher frequencies at full power with the existing set-up. A total of 60 trains with 360 pulses were delivered per 30-minute TMS treatment. An air-cooled double coil was used which has opposite current directions in each coil, generating magnetic fields on top side of each coil with opposite directions. Using air-cooled coils allowed us to induce magnetic fields without raising the temperature of the T-75 flasks placed on them. All TMS treatments on N27 cells were performed in a sterile biosafety cabinet (Fig. 9). The flask set above the left coil was designated “Field up” and the flask set above the right coil was designated “Field down”, corresponding to the orientation of the magnetic fields.

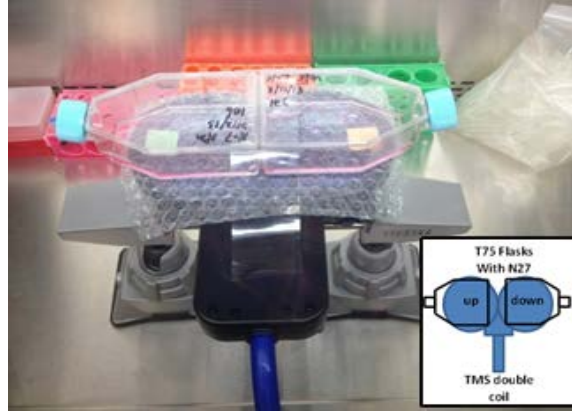


Fig. 9 Arrangement of the 30-minute TMS treatment delivered to two T-75 flasks. The directions of the two oppositely oriented magnetic fields were labeled on the double coil. Field orientation was upward on the left coil and downward on the right coil, as shown in the inset figure. We used two clamps to fix the coil in the cell culture cabinet and a layer of bubble wrap separated both flasks from the coils to maintain a thermal barrier.

D. Cytotoxicity assay

Cytotoxic cell death was measured as per Life Technologies' Trypan blue exclusion cell counting method [15]. Briefly, after treatment cells were harvested with trypsin-EDTA and resuspended in 1X PBS, we then took 10 μ l of cell suspension from one sample and added with 10 μ l of 0.4% trypan blue solution (Life Technologies). Then, we put 10 μ l of the mixture into the cell counting slide and place the slide into the automatic cell counter to count the concentration of cells in each sample. Finally, we extrapolated the total number of cells in each sample by multiplying its volume and concentration [15]. By using this method, we counted the number of cells in each of the four replicate samples according to the counting time points shown in Table. I. We studied the effect of TMS on 2 different initial cell densities, 1 million cells/flask and 0.5 million cells/flask (n=4).

Table 1. Design of the TMS experiment with Trypan blue cell counting method for cell densities of 1 and 0.5 million cells /flask.

Culture Time point	Counting Time point	Sample Description			
		Incubator	Environmental	Field up	Field down
Day 0	Day 1	Incubator	Environmental	Field up	Field down
Day 0.5	Day 1.5	Incubator	Environmental	Field up	Field down
Day 1	Day 2	Incubator	Environmental	Field up	Field down
Day 1.5	Day 2.5	Incubator	Environmental	Field up	Field down
Day 2	Day 3	Incubator	Environmental	Field up	Field down

Table 2. Design of the TMS experiment with CyQuant cell viability assay cell counting method for cell densities of 100k, 80k, 50k and 20k per well

Culture Time Point	Counting Time point	Sample Description		
		Environmental	Field up	Field down
Day 0	Day 1	Environmental	Field up	Field down
Day 1	Day 2	Environmental	Field up	Field down
Day 2	Day 3	Environmental	Field up	Field down

E. *CyQuant cell proliferation assay*

We used Life technologies' CyQuant cell viability assay to confirm our results from the Trypan blue cell counting procedures. On day 0, we seeded the N27 cells in 24-well plates (n=3) with the four rows per plate. In each plate, there were 4 rows and three columns. Row 1 to row 4 have different seeding densities; 20k, 50k, 80k, to 100k, respectively. Each row had three replicated samples in three columns to account for standard deviation. We had three groups with different culture times: Day 0, Day 1 and Day 2 (Table II). Briefly, after 24

hours post-treatment, we read the fluorescence with excitation maximum at 485 nm and the emission maximum at 530 nm using a Synergy 2 plate reader (BioTek) [16]. We pooled the groups designated as Incubator and Environmental in Table I, because the difference between them was insignificant.

F. MTS cell viability assay cell counting method

Cell viability was measured using Promega's MTS assay to confirm the results from Trypan blue and CyQuant cell proliferation assays. Briefly, on day 0, we seeded the wells of 96-well plates with 15k for one row and half with 20k for another row of N27 cells in 200 μ L of proliferation medium per well. Each row had 6 duplicated samples (n=6). The design of the experiment was according to Table III., TMS treatment was performed with "Field up" and "Field down" on 2 different well plates. After 24 hours post-treatment, 20 μ l MTS reagent (CellTiter 96® Aqueous One Solution Reagent) was added to each well and incubated at 37°C in a CO₂ incubator for 90 min and absorbance was read at 490 nm and 670 nm in a Spectramax plate reader (Molecular Devices). We subtracted the baseline via Abs₄₉₀-Abs₆₇₀ prior to data analysis [17].

Table 3. Design of the TMS experiment with MTS cell viability assay cell counting method for cell densities of 15k and 20k per well.

Culture Time Point	Counting Time point	Sample Description			
		Control	Environmental	Field up	Field down
Day 0	Day 1				

G. Statistical significance analysis

Statistical significance analysis was performed using Originlab 9.0 software (OriginLab Corporation, Northampton, MA, USA). Raw data analysis were analyzed using a

two unpaired t-test. Statistically significant differences are indicated by asterisks as follows: * $p < 0.05$, ** $p < 0.01$ and *** $p < 0.001$.

Results

After TMS treatment of N27 cells, we counted the number of viable cells using the Trypan blue method for initial seeding densities of 1 million (Fig. 10) and 0.5 million (Fig. 11) cells per flask. The culture time and counting time points are indicated in Table I. The result showed that the proliferation rate increased after TMS stimulation with the magnetic field oriented upward through the horizontal plane of adherent cells, compared to incubator and environmental samples. The proliferation rate decreased when the field was oriented downward through the horizontal growth plane compared to incubator and environmental samples. Also, environmental samples exhibited slower proliferation compared to the incubator condition. For the lower seeding density (Fig.11), the difference of cell counting for each group became larger over time. The difference peaked on Day 3 when the number of cells in the “Field up” group was $23.57 \pm 3.21\%$ (mean \pm STD, *** $p < 0.001$) higher than that in the Environmental group, while in the Field down group, it was $11.45 \pm 1.99\%$ (** $p < 0.001$) lower than in the Environmental group. Therefore, the total difference in cell’s proliferation rate attributable to TMS field direction was +35.02 %.

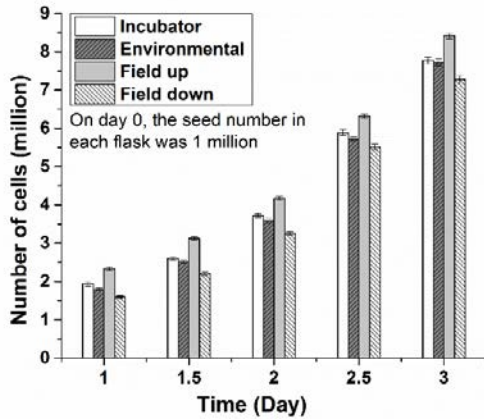


Fig. 10 Cell densities in the TMS experiment, derived using the Trypan blue cell counting method with an initial seeding density of 1 million cells/flask. Counting time is indicated in Table. I.

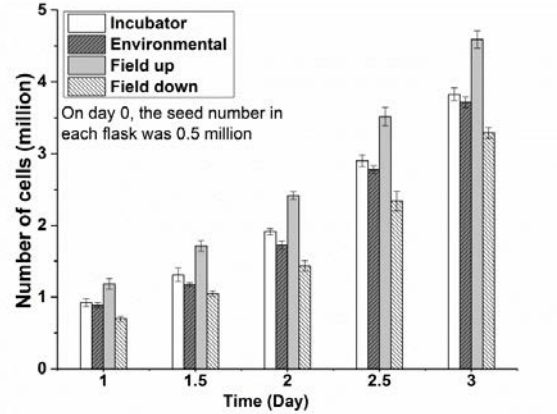


Fig. 11 Cell densities in the TMS experiment, derived using the Trypan blue cell counting method with initial seeding density of 0.5 million cells/flask. Counting time is indicated in Table. I.

To investigate the effect of different culture times on cell proliferation, we conducted another experiment expanding culture time from 2 days to 2.5 days. The seeding density was 0.5 million/flask and the new culture time points were Day 0.5, Day 1, Day 1.5, Day 2 and Day 2.5. Cells were counted 24 h after each treatment, so the corresponding counting time points were Day 1.5, Day 2, Day 2.5, Day 3 and Day 3.5 respectively. The effect of TMS and its direction on the proliferation of cells over time (Fig. 12) was similar to the previous results for this seeding density (Fig. 11). On Day 3.5, the number of cells in the “Field up” group was $13.53 \pm 1.36\%$ (** $p < 0.001$) higher than in the Environmental group, whereas the number of cells in the “Field down” group was $12.61 \pm 1.76\%$ (** $p < 0.001$) lower than in the Environmental group. Therefore, the total difference in cell’s proliferation rate attributable to TMS field direction was +26.14 %.

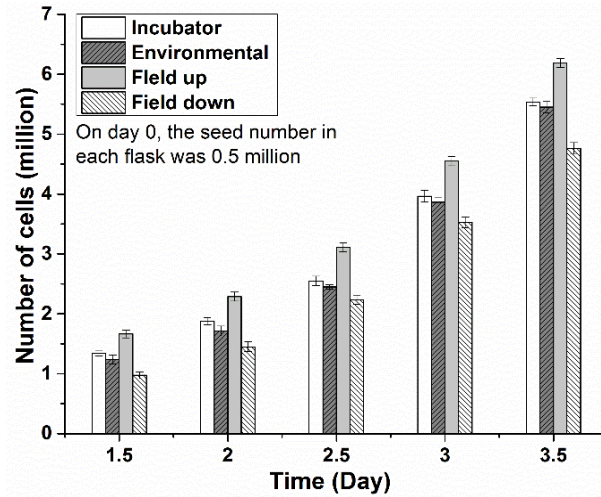


Fig.12 Cell densities in the TMS experiment, derived using the Trypan blue cell counting method for an initial seeding density of 0.5 million cells/flask. Culture times were Day 0.5, Day 1, Day 1.5, Day 2 and Day 2.5. The corresponding Counting times were Day 1.5, Day 2, Day 2.5, Day 3 and Day 3.5, respectively.

We used the CyQuant cell viability assay to confirm the results obtained with the Trypan blue cell counting method. This time we eliminated group 1 (Incubator) and we set four seeding densities. The design of this experiment was based on Table II. The effect of TMS field direction on cell proliferation obtained via the CyQuant method (Fig 13-16) was similar to the effect measured using the Trypan blue cell counting method. However, Fig.8, which had the seeding density of 100k per well did not follow the trend similar to other seeding densities i.e. the difference in the proliferation rate was not pronounced. It may be due to the fact that a large number of cells grew in the limited space so the cells might have attained 100% confluency earlier than Day 3.

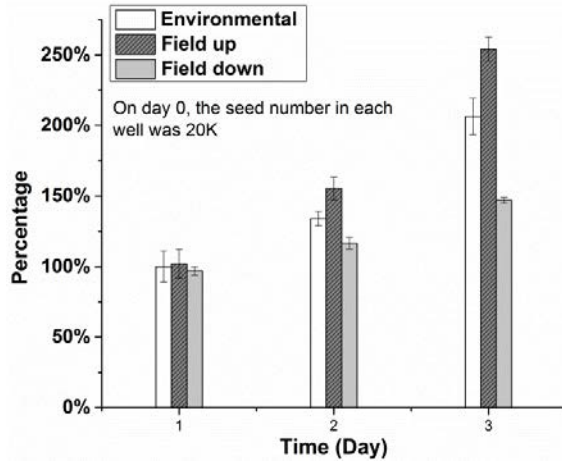


Fig. 13 Cell proliferation after TMS treatment of plates with an initial seeding density of 20k/well. We used the CyQuant cell viability assay to count cells. On day 3, the number of cells in the “Field up” group was $22.06 \pm 4.14\%$ (mean \pm STD as a percentage of the initial seeding density, $*p < 0.05$) higher than in the Environmental group, whereas cell numbers in the “Field down” group were $28.77 \pm 1.00\%$ ($**p < 0.01$) lower than in the Environmental group.

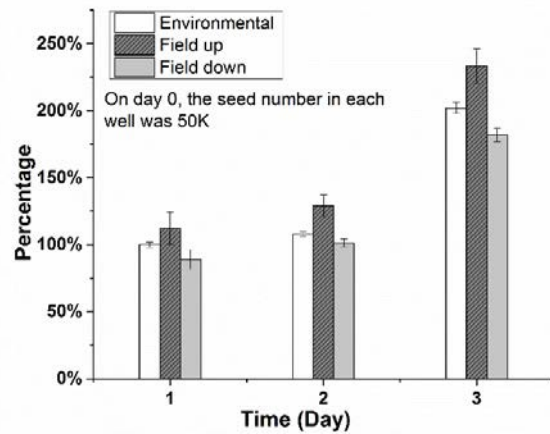


Fig.14 Cell proliferation after TMS treatment of plates with an initial seeding density of 50k/well. We used the CyQuant cell viability assay to count cells. On day 3, the number of cells in the “Field up” group was $15.49 \pm 7.26\%$ (mean \pm STD as a percentage of the initial seeding density, $*p < 0.05$) higher than in the Environmental group, whereas cell numbers in the “Field down” group were $9.94 \pm 2.47\%$ ($*p < 0.05$) lower than in the Environmental group.

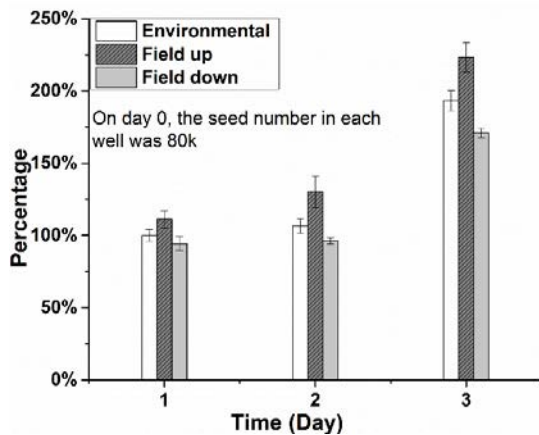


Fig.15 Cell proliferation after TMS treatment of plates with an initial seeding density of 80k/well. We used the CyQuant cell viability assay to count cells. On day 3, the number of cells in the “Field up” group was $15.57 \pm 5.17\%$ (mean \pm STD as a percentage of the initial seeding density, $*p < 0.05$) higher than in the Environmental group, whereas cell numbers in the “Field down” group were $11.62 \pm 1.55\%$ ($*p < 0.05$) lower than in the Environmental group.

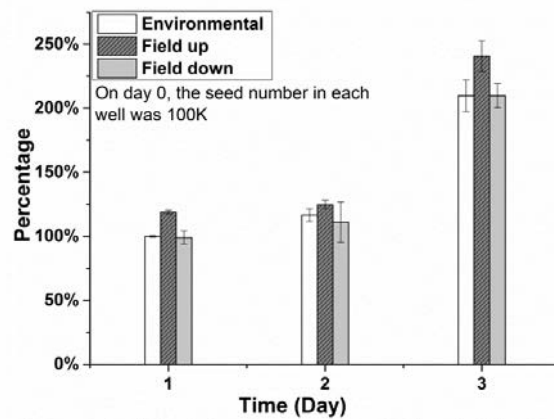


Fig.16 Cell proliferation after TMS treatment of plates with an initial seeding density of 100k/well. We used the CyQuant cell viability assay to count cells. On day 3, the number of cells in the “Field up” group was $14.69 \pm 5.74\%$ (mean \pm STD as a percentage of the initial seeding density, $p > 0.05$) higher than in the Environmental group, whereas cell numbers in the “Field down” group were the same ($0 \pm 4.50\%$, $p > 0.05$) as those in the Environmental group.

A third cell counting method, the MTS cell viability assay, was performed to confirm the results obtained with the Trypan blue and CyQuant cell counting methods. With an initial seeding of 15k (Fig. 17), the number of cells in the “Field up” group was $19.88 \pm 4.56\%$ (** $p < 0.001$) higher than in the Environmental control group. Meanwhile, the number of cells in the “Field down” group was $8.88 \pm 1.39\%$ (** $p < 0.01$) lower than in the Environmental group. Next, using an initial seeding of 20k (Fig. 18), the number of cells in the “Field up” group was $19.60 \pm 4.57\%$ (** $p < 0.01$) higher than in the Environmental group, while the number of cells in the “Field down” group was $8.16 \pm 0.09\%$ (** $p < 0.01$) lower than in the Environmental group. Therefore, the total difference in cell’s proliferation rate attributable to TMS field direction was $+27.76\%$.

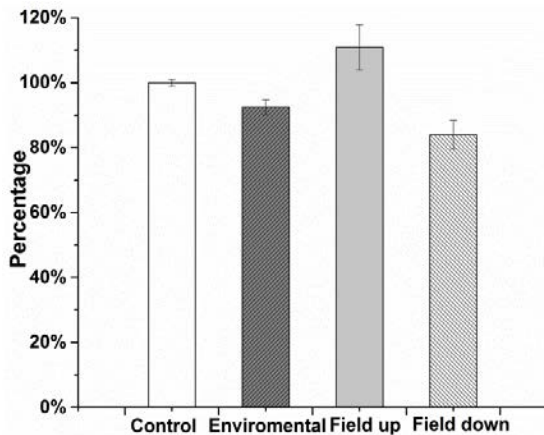


Fig. 17 Cell proliferation after TMS treatment of plates with an initial seeding density of 15k/well. We used the MTS cell viability assay to count cells, reported here as a percentage of control group1 (Incubator).

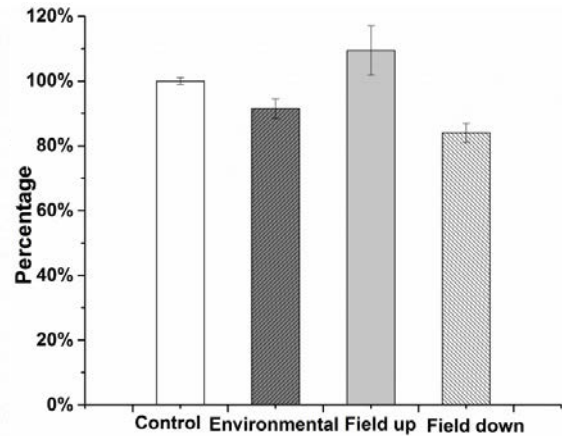


Fig. 18 Cell proliferation after TMS treatment of plates with an initial seeding density of 20k/well. We used the MTS cell viability assay to count cells, reported here as a percentage of control group1 (Incubator).

Discussion

We investigated the effect of magnetic field orientation on the proliferation rate of N27 dopaminergic neuronal cells using three different cell counting methods to cross-validate

the results. The MTS assay showed the highest difference in cell proliferation rate. It was also easy to replicate this counting procedure three times to obtain standard deviation. In the Trypan blue cell counting method, we used flasks to culture neuronal cells, which required more area to incubate replicate samples. Cell counting using the Trypan blue method was more time consuming because cell counting was performed one flask at a time, unlike the MTS method where cell counting was performed in groups. There were three replicate samples for each group (n=3) for Trypan blue method and for MTS and CyQuant cell viability assay, n=6, which is adequate to show statistical significance. In the CyQuant cell viability cell counting method, it was easy to replicate samples and we were also able to count cells of all groups at once, but the differences among groups were slightly smaller than those from the MTS cell counting method. Thus, the MTS cell viability assay cell counting method is recommended for investigating the proliferation rate of N27 dopaminergic neuronal cells under TMS treatment.

According to the design of all these experiments, each group of N27 dopaminergic neuronal cells received a 30 minutes TMS treatment each day. After experimenting with a one-hour treatment, we found that increasing the treatment time did not make much difference on cell proliferation rate. We used 0.25 Hz as the actual frequency because the minimum discharging and recharging time for the capacitor is 4 seconds when we set intensity of the monophasic stimulator at 100%. This time can be reduced by setting a lower intensity. However, we have used 100% intensity in order to have significant effect on the growth/proliferation rate. The temperature on the coil surfaces was measured by a thermal sensor which showed the temperature of the coil during stimulation. A temperature of 21.7 ± 0.1 °C was maintained in the flask and throughout the stimulation period. There was no

obvious vibration of coils during the stimulation discerned by visually since the coil was fixed by two stages. Therefore, the difference in neural proliferation rate was due to the different orientation of magnetic field generated by double coil. Since during TMS the corresponding electric field generated by time varying magnetic field can affect neurons firing rate [9], different orientation of magnetic field generated clockwise and counterclockwise electric fields and induced current in the brain. The difference in the sequence of clockwise and counterclockwise induced eddy current in the neurons is the reason for the different proliferation of neurons. Since, the interaction between magnetic field and neurons is not well established, further investigation of changes in neuron responses due to application of time varying magnetic fields such as TMS are warranted.

We plan to use different types of neuronal cells in future experiments to assess whether our results were cell-specific. We will also employ advanced imaging techniques to investigate any morphological changes in cells and cell components due to the effect of magnetic field orientation and stimulus parameters. Many factors potentially impact the proliferation of neuronal cells, such as BDNF, GDNF and NGF [18] so we will investigate the effects of TMS fields on these growth proteins.

Conclusions

The effect of magnetic field direction generated by TMS coils on the proliferation of N27 dopaminergic neuronal cells was investigated. Orienting the magnetic field upward through the horizontal plane of adherent cells increased their proliferation rate while orienting the magnetic field downward through the cell growth plane decreased their proliferation rate. The results obtained by the Trypan blue method of cell counting was verified by the CyQuant and MTS cell viability assay methods and all the results are

statistically significant. The changes in cell proliferation rate due to magnetic field direction is an important step forward in understanding the effect of magnetic fields on neuronal cell biology. Our findings could have important implications for the preclinical development of TMS treatments of neurological disorders and represents a new method to control the proliferation rate of neuronal cells.

References

- [1] Barker AT, Jalinous R, Freeston IL. Non-invasive magnetic stimulation of human motor cortex. *Lancet* 1985;325:1106–7. doi:10.1016/S0140-6736(85)92413-4.
- [2] George MS, Lisanby SH, Sackeim HA. Transcranial Magnetic Stimulation. *Arch Gen Psychiatry* 1999;56:300. doi:10.1001/archpsyc.56.4.300.
- [3] Vonloh M, Chen R, Kluger B. Safety of transcranial magnetic stimulation in Parkinson's disease: a review of the literature. *Parkinsonism Relat Disord* 2013;19:573–85. doi:10.1016/j.parkreldis.2013.01.007.
- [4] Rosenberg PB. Repetitive Transcranial Magnetic Stimulation Treatment of Comorbid Posttraumatic Stress Disorder and Major Depression. *J Neuropsychiatr* 2002;14:270–6. doi:10.1176/appi.neuropsych.14.3.270.
- [5] Dodick DW, Schembri CT, Helmuth M, Aurora SK. Transcranial magnetic stimulation for migraine: a safety review. *Headache* 2010;50:1153–63. doi:10.1111/j.1526-4610.2010.01697.x.
- [6] Crowther LJ, Hadimani RL, Jiles DC. A numerical dosimetry study for pediatric transcranial magnetic stimulation. 2013 6th Int. IEEE/EMBS Conf. Neural Eng., IEEE; 2013, p. 239–42. doi:10.1109/NER.2013.6695916.
- [7] Wassermann EM, Zimmermann T. Transcranial magnetic brain stimulation: therapeutic promises and scientific gaps. *Pharmacol Ther* 2012;133:98–107. doi:10.1016/j.pharmthera.2011.09.003.
- [8] March S, Stark S, Hadimani M, Stiner D, Senter M, Spoth K, et al. Thermal and Mechanical Analysis of Novel Transcranial Magnetic Stimulation Coil for Mice. *IEEE Trans Magn* 2014;PP:1–1. doi:10.1109/TMAG.2014.2316479.

- [9] Bonmassar G, Lee SW, Freeman DK, Polasek M, Fried SI, Gale JT. Microscopic magnetic stimulation of neural tissue. *Nat Commun* 2012;3:921. doi:10.1038/ncomms1914.
- [10] Miyakoshi J. Effects of static magnetic fields at the cellular level. *Prog Biophys Mol Biol* 2005;87:213–23. doi:10.1016/j.pbiomolbio.2004.08.008.
- [11] Ariza CA, Fleury AT, Tormos CJ, Petruk V, Chawla S, Oh J, et al. The influence of electric fields on hippocampal neural progenitor cells. *Stem Cell Rev* 2010;6:585–600. doi:10.1007/s12015-010-9171-0.
- [12] Gaetani R, Ledda M, Barile L, Chimenti I, De Carlo F, Forte E, et al. Differentiation of human adult cardiac stem cells exposed to extremely low-frequency electromagnetic fields. *Cardiovasc Res* 2009;82:411–20. doi:10.1093/cvr/cvp067.
- [13] Anantharam V, Kitazawa M, Wagner J, Kaul S, Kanthasamy AG. Caspase-3-dependent proteolytic cleavage of protein kinase Cdelta is essential for oxidative stress-mediated dopaminergic cell death after exposure to methylcyclopentadienyl manganese tricarbonyl. *J Neurosci* 2002;22:1738–51.
- [14] Prasad KN, Clarkson ED, Rosa FG La, Edwards-prasad J, Freed CR. MINIREVIEW Efficacy of Grafted Immortalized Dopamine Neurons in an Animal Model of Parkinsonism : A Review 1998;9:1–9.
- [15] Xu Q, Kanthasamy AG, Reddy MB. Neuroprotective effect of the natural iron chelator, phytic acid in a cell culture model of Parkinson's disease. *Toxicology* 2008;245:101–8. doi:10.1016/j.tox.2007.12.017.
- [16] Jones LJ, Gray M, Yue ST, Haugland RP, Singer VL. Sensitive determination of cell number using the CyQUANT® cell proliferation assay. *J Immunol Methods* 2001;254:85–98. doi:10.1016/S0022-1759(01)00404-5.
- [17] Mahon X, Deininger MWN, Schultheis B, Reiffers J, Goldman JM, Melo J V. Selection and characterization of BCR-ABL positive cell lines with differential sensitivity to the tyrosine kinase inhibitor STI571 : diverse mechanisms of resistance *Franc* 2000;96:1070–9.
- [18] Allen SJ, Watson JJ, Shoemark DK, Barua NU, Patel NK. GDNF, NGF and BDNF as therapeutic options for neurodegeneration. *Pharmacol Ther* 2013;138:155–75. doi:10.1016/j.pharmthera.2013.01.004.

CHAPTER 3. THERMAL AND MECHANICAL ANALYSIS OF VARIABLE TMS COIL SYSTEM

Modified from a paper published in *Journal of Applied Physics*, vol. 117, no. 17, p. 17B305, 2015

Y. Meng, R. L. Hadimani, L. J. Crowther, Z. Xu, J. Qu, and D. C. Jiles
Department of Electrical and Computer Engineering, Iowa State University, Ames IA 50011, US

Abstract

Transcranial Magnetic Stimulation (TMS) has the potential to treat various neurological disorders non-invasively and safely. The “Halo coil” configuration can stimulate deeper regions of the brain with lower surface to deep-brain field ratio compared to other coil configurations. The existing “Halo coil” configuration is fixed and is limited in varying the site of stimulation in the brain. We have developed a new system based on the current “Halo coil” design along with a graphical user interface (GUI) system that enables the larger coil to rotate along the transverse plane. The new system can also enable vertical movement of larger coil. Thus, this adjustable “Halo coil” configuration can stimulate different regions of the brain by adjusting the position and orientation of the larger coil on the head. We have calculated magnetic and electric fields inside an MRI-derived heterogeneous head model for various positions and orientations of the coil. We have also investigated the mechanical and thermal stability of the adjustable “Halo coil” configuration for various positions and orientations of the coil to ensure safe operation of the system.

Introduction

Transcranial magnetic stimulation (TMS) is a painless and non-invasive neuromodulation technique based on the principles of magnetic induction [1-2]. TMS has been used to study brain function and is being investigated as a possible treatment for

numerous brain disorders [3]. The technique already shows good efficacy for the treatment of major depressive disorder [4]. We have previously reported a “Halo coil” configuration which can stimulate deeper regions of the human brain, but the configuration was fixed so that only a single site in the brain has a lower surface to deep-brain field ratio compared to other coil configurations [5]. Now, we have built a variable “Halo coil” configuration with a circular coil fixed on top of the head and with vertical and rotational movement of the larger coil to selectively stimulate different regions of the brain. During the stimulation, we used two stimulators to send AC current signals to two coils. One stimulator sends an AC current with a frequency of 2.5 kHz and an amplitude of 2500 A to the circular coil. The other stimulator sends AC current with a frequency of 2.5 kHz and an amplitude of 5000 A to the larger coil. We have also conducted thermal and mechanical analysis of the system to ensure its feasibility and stability. A GUI system has been built that accurately controls the movement and rotation of the larger coil using an Arduino microcontroller.

Magnetic (Lorentz) Force Response

COMSOL Multiphysics (Los Angeles, CA, USA) was used for magnetic force analysis. A 5000 A DC current was assigned in both coils to evaluate the maximum forces induced on the variable “Halo coil” system. Any forces experienced by the coils will be transferred to the insulation and thus the yield strength of insulation should be higher than the Lorentz forces exerted by the magnetic fields generated by the coils. The yield strength of copper is 70 MPa [6] and the ultimate tensile strength of the insulation, Nylon is 125 MPa [7]. The Lorentz force density in the coil can be calculated by equation (4), where J [A/m] is the current density and B [T] is the magnetic flux density. In this study, we used 3D models where J [A/m³] is the current density and $i = x, y, z$.

$$\mathbf{f}_i = \mathbf{J} \times \mathbf{B} \quad (4)$$

The calculated Lorentz force density f [N/m^3] is shown in Fig. 3 for two extreme conditions for our system. The larger coil is rotated $+30^\circ$ and the distance between the centers of two coils is 5 cm and 15 cm. Fig. 19 (a) is the top view, (b) is the side view for a distance of 5 cm between the coils. In Fig. 19 (c) and (d), the distance between the centers of two coils is 15 cm, (c) is the top view, (d) is the side view.

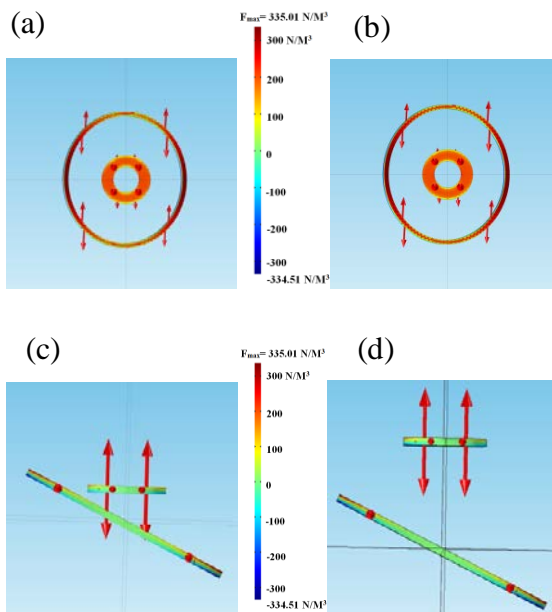


Fig. 19 The result of force analysis between the two coils with larger coil rotated at $+30^\circ$. In (a) and (b), the distance between the centers of two coils is 5 cm, while (a) is the top view, (b) is the side view. In (c) and (d), the distance between the centers of two coils is 15 cm, while (c) is the top view, (d) is the side view.

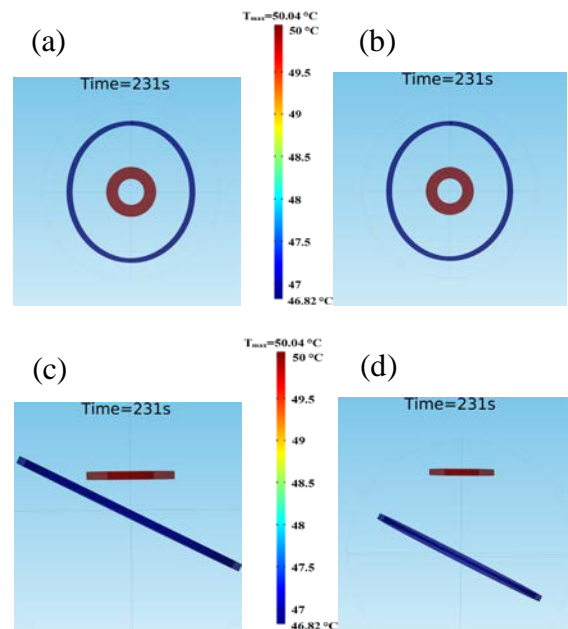


Fig. 20 The result of thermal analysis of two coils with larger coil rotated at $+30^\circ$. In (a) and (b), the distance between the centers of two coils is 5 cm, while (a) is the top view, (b) is the side view. In (c) and (d), the distance between the centers of two coils is 15 cm, while (c) is the top view, (d) is the side view.

The arrows in the picture show the direction of Lorentz forces and their lengths indicate the magnitude of that force density. In the side view, the majority of Lorentz force density was parallel to the direction of vertical movement of the large coil. The maximum

Lorentz force was 335.01 MN/m^3 . The equivalent stress on the larger coil was 3.35 MPa . The coils are made of copper with a yield strength of 70 MPa and covered with Nylon, which has a yield/ultimate tensile strength of 125 MPa . Thus, the stress due to the Lorentz forces in the larger coil was significantly smaller than the yield strength of copper and Nylon. The system is therefore be mechanically stable and can withstand the expected Lorentz forces. However, the cyclic loading conditions which can occur in repetitive TMS have not been analyzed.

Thermal Analysis

The temperature in the coils was another important factor in the system because of the high amplitude of the current induced in the coil. This can generate a large amount of heat in the coil due to Joule's law ($Q = I^2 \cdot R \cdot t$). The limit of surface temperature for electrical medical equipment has been specified by General Standard IEC 60601-2-37, which is 50°C in air and 43°C at the surface of the body [8]. Thus, the modeling of heat was focused on the duration of the stimulation when either of the coils reached 50°C . The incompressible Navier-Stokes heat equation from the COMSOL Heat Transfer module was used to model the thermal changes in the coil system under TMS therapy conditions, as shown equation (5),

$$\rho C_p \frac{\partial T}{\partial t} + C_p \mathbf{u} \cdot \nabla T = \nabla \cdot (k \nabla T) + Q \quad (5)$$

where ρ is the fluid density, C_p is the fluid heat capacity, T is the temperature, \mathbf{u} is the velocity field of the fluid, k is the thermal diffusivity of the material, and Q is external source heating [9]. According to the modeling results shown in Fig. 20, after stimulation for 231 seconds, the small circular coil which is placed on the top on patient's head, reached 50.04°C . Additionally, the vertical position and the rotational movement of the larger coil did not

have a significant effect on the heat generated in the two coils as all positions and orientations demonstrated similar results of approximately 50 °C in the smaller coil after 231 seconds of stimulation.

GUI system

A graphical user interface (GUI) was developed in Java to control the movement and rotation of the larger coil with a computer via an Arduino microcontroller as shown in Fig. 21. The left portion of the interface is the control

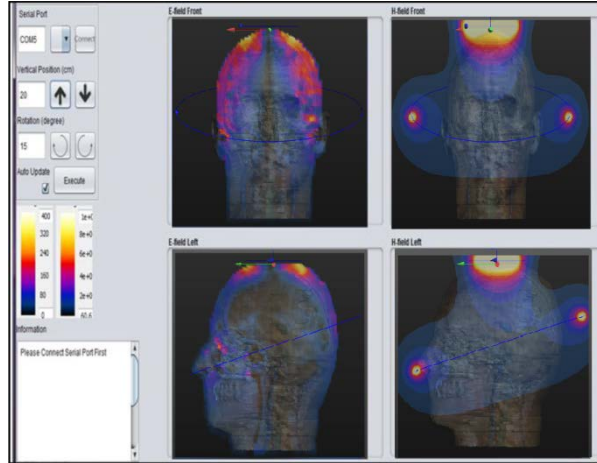


Fig. 21 The graphic user interface (GUI)

panel which has two buttons to control the vertical movement of large coil by a linear actuator. The range of vertical movement is -5 cm to +5 cm compared to its origin with a step size of 1 cm. It also has two buttons to control the rotation by a servo motor. The range of rotation is -30° to +30° compared to its origin with a step size of 5°. The right portion of the interface shows the modeling results of electric and magnetic field for the selected position of the large coil. These images will show the distribution of magnetic and electric field which will indicate the site of stimulation with a field larger than the threshold or peak field for the selected position of the large coil.

Conclusion

TMS is a novel non-invasive and safe treatment for various neurological disorders. In our present work, we have designed and developed a variable “Halo coil” system that can

achieve deep brain stimulation at specific treatment areas with the vertical and rotational movement of the larger coil in the “Halo coil” system. We have also developed a GUI system to control the movement precisely via a computer. The modeling results of magnetic and electric field confirm that our design can stimulate different parts of human brain. The modeling result of Lorentz forces show that the magnetic forces in coils do not exceed the yield strengths of the coil material and casing in the system. The modeling results of Joule heating showed that the treatment time of 231 seconds will heat the coil to a temperature of 50.04 °C. Thus for longer treatment times, an active cooling system using external air or water circulation should be considered.

References

- [1] A. T. Barker, I. L. Freeston, R. Jalinous, and J. A. Jarratt, “Motor responses to non-invasive brain stimulation in clinical practice,” *Electroencephalogr. Clin. Neurophysiol.*, vol. 61, no. 3, p. S70 –, 1985.
- [2] P. J. Basser and B. J. Roth, “Stimulation of a myelinated nerve axon by electromagnetic induction,” *Medical & Biological Engineering & Computing*, vol. 29, no. 3, pp. 261–268, 1991.
- [3] S. Rossi, M. Hallett, P. M. Rossini, and A. Pascual-Leone, “Safety, ethical considerations, and application guidelines for the use of transcranial magnetic stimulation in clinical practice and research.,” *Clin. Neurophysiol.*, vol. 120, no. 12, pp. 2008–39, Dec. 2009.
- [4] M. S. George, S. H. Lisanby, D. Avery, W. M. McDonald, V. Durkalski, M. Pavlicova, B. Anderson, Z. Nahas, P. Bulow, P. Zarkowski, P. E. Holtzheimer, T. Schwartz, and H. A. Sackeim, “Daily left prefrontal transcranial magnetic stimulation therapy for major depressive disorder: a sham-controlled randomized trial.,” *Arch. Gen. Psychiatry*, vol. 67, no. 5, pp. 507–16, May 2010.

- [5] L. J. Crowther, P. Marketos, P. I. Williams, Y. Melikhov, D. C. Jiles, and J. H. Starzewski, "Transcranial magnetic stimulation: Improved coil design for deep brain investigation," *J. Appl. Phys.*, vol. 109, no. 7, pp. 2009–2012, 2011.
- [6] L. J. Crowther, K. Porzig, R. L. Hadimani, H. Brauer, and D. C. Jiles, "Realistically Modeled Transcranial Magnetic Stimulation Coils for Lorentz Force and Stress Calculations During MRI," *IEEE Trans. Magn.*, vol. 49, no. 7, pp. 3426–3429, Jul. 2013.
- [7] H. Mahfuz, A. Adnan, V. K. Rangari, M. M. Hasan, S. Jeelani, W. J. Wright, and S. J. DeTeresa, "Enhancement of strength and stiffness of Nylon 6 filaments through carbon nanotubes reinforcement," *Appl. Phys. Lett.*, vol. 88, no. 8, p. 083119, 2006.
- [8] IEC IS 60601: Medical Electrical Equipment -- Part 2–37, (2005).
- [9] S. March, S. Stark, M. Hadimani, D. Stiner, M. Senter, K. Spoth, L. Crowther, and D. Jiles, "Thermal and Mechanical Analysis of Novel Transcranial Magnetic Stimulation Coil for Mice," *IEEE Trans. Magn.*, vol. PP, no. 99, pp. 1–1, 2014.

CHAPTER 4.GENERAL CONCLUSIONS

General Discussion

The study in Chapter 2 has investigated the effect of different orientation of magnetic field for TMS on the proliferation rate of N27 dopamine cells. Basically, the proliferation rate of N27 cells would increase after being treated with the magnetic field orienting upward through the horizontal plane of adherent cells while the rate would decrease after being treated with the magnetic field orienting downward through the cell growth plane. It also compared the advantages of three different cell counting methods which could give a suggestion to related studies in future. The result of this study would bring more attention on the in-vitro and in-vivo study on TMS to understand its mechanism or its effect on neural cells or tissues.

The result in Chapter 3 has demonstrated the stability and feasibility of the Variable TMS coil system. It shows that the maximum electromagnetic (Lorentz) force was much smaller than the yield strength of the coil and its cover materials. Meanwhile, it points out the maximum time for treatment using this system is 231 seconds or 3 minutes and 51 seconds because of one of coils in the system would reach 50 °C at that time, which is the highest temperature for electrical medical equipment according to General Standard IEC 60601-2-37. Moreover, the vertical and rotational movement of the Halo coil does not affect both the mechanical and thermal properties of the whole system, which shows its stability.

The results in chapter 2 and chapter 3 are addressed two major research areas in-vitro study and computer modeling and coil design, respectively. The results could help us to investigate more of the basic mechanism of TMS and bring more efficient and compact tools in clinical trials. Therefore, there are many promising research opportunities in TMS in the

three major areas shown in Fig. 2, which would eventually bring TMS as a major tool to treat different kinds of human brain diseases.

Recommendation for Future Research

Although the results in chapter 2 have shown the effect of magnetic field on proliferation rate of neurons, the basic mechanism of how TMS influences the growth of neurons is still not understood. In the meantime, there are many factors that could affect cell's growth such as temperature, electromagnetic force, gravity and certain proteins like BDNF, GDNF and NGF [1]. Since we have monitored and demonstrated that temperature and electromagnetic force did not contribute much to the results in the experiment. Future work can be done on analysis those proteins like BDNF, GDNF and NGF. Besides, some articles have shown effect of magnetic field on the soma size and axon length of neural cells and using magnetic field to direct axon growth [2-3]. Thus, morphology studies on neurons by TMS treatment would be another approach to investigate its mechanism. Moreover, magnetic nanoparticles have shown possibilities for cell recognition, isolation, purification and enhancing the effect of magnetic field [3-4], so using magnetic nanoparticles in the experiment could show more significant results.

The heat issue of TMS coil is one main challenge for long time repetitive TMS (rTMS) treatment. In our variable TMS coil system, the maximum treating time is less than 4 minutes, which is quite small compared to treating time of regular repetitive TMS treatment. Although this issue can be resolved by adding water-cooling or air-cooling to the coil [5], the cooling component highly increases the weight of the coil which makes it difficult to build enough support structure for vertical and rotational movement of the coil. In our current design, we used polymer and 3D printing technology to make the support structure. However,

it cannot support the heavy cooling component of the coil, so future work can be done on design a more firm support structure to hold the air-cooling coil for long time TMS treatment with the variable TMS coil system.

References

- [1] S. J. Allen, J. J. Watson, D. K. Shoemark, N. U. Barua, and N. K. Patel, “GDNF, NGF and BDNF as therapeutic options for neurodegeneration.,” *Pharmacol. Ther.*, vol. 138, no. 2, pp. 155–75, May 2013.
- [2] S. Kim, W. S. Im, L. Kang, S. T. Lee, K. Chu, and B. I. Kim, “The application of magnets directs the orientation of neurite outgrowth in cultured human neuronal cells,” *J. Neurosci. Methods*, vol. 174, no. 1, pp. 91–96, 2008.
- [3] C. Riggio, M. P. Calatayud, M. Giannaccini, B. Sanz, T. E. Torres, R. Fernández-Pacheco, A. Ripoli, M. R. Ibarra, L. Dente, A. Cuschieri, G. F. Goya, and V. Raffa, “The orientation of the neuronal growth process can be directed via magnetic nanoparticles under an applied magnetic field,” *Nanomedicine Nanotechnology, Biol. Med.*, vol. 10, no. 7, pp. 1549–1558, 2014.
- [4] C. Ooi, C. M. Earhart, R. J. Wilson, and S. X. Wang, “Effect of Magnetic Field Gradient on Effectiveness of the Magnetic Sifter for Cell Purification,” vol. 49, no. 1, pp. 316–320, 2013.
- [5] L. G. Cohen, P. Celnik, A. Pascual-Leone, B. Corwell, L. Falz, J. Dambrosia, M. Honda, N. Sadato, C. Gerloff, M. D. Catalá, and M. Hallett, “Functional relevance of cross-modal plasticity in blind humans.,” *Nature*, vol. 389, no. 6647, pp. 180–183, 1997.

APPENDIX A. MODELING OF ELETRIC AND MAGNETIC FIELD FOR VARIABLE TMS COIL SYSTEM

We have used SEMCAD X (SPEAG, Swiss) finite element software to calculate the electric and magnetic fields generated by the fixed circular coil positioned at the vertex of the head with different orientations of the larger coil. An AC current with a frequency of 2.5 kHz and an amplitude of 2500 A was applied to the circular coil which is comparable to the pulse signal generated by a biphasic commercial TMS stimulator with 50% power intensity, and a current signal of the same frequency but with an amplitude of 5000 A was applied to the large coil [1]. We have used an anatomically realistic human head model with different electrical properties assigned to each tissue of the brain [2]. These parameters are shown in Table I [3].

Table 4. Values of Dielectric Properties at 2.5 kHz

Tissue	ϵ_r (Relative Permittivity)	σ (Electric Conductivity) [S/m]
Brain (grey matter)	7.81×10^4	1.04×10^{-1}
Brain (white matter)	3.43×10^4	6.45×10^{-2}
Cerebellum	7.84×10^4	1.24×10^{-1}
Cerebrospinal fluid	1.09×10^2	2.00
Skin	1.14×10^3	2.00×10^{-4}
Skull	1.44×10^3	2.03×10^4

The calculation of magnetic field was based on the Biot-Savart law as shown in equation (1) [4].

$$\mathbf{A}_0(\mathbf{r}) = \frac{\mu_0}{4\pi} \int_{\Omega} \frac{\mathbf{J}_0(\mathbf{r}')}{|\mathbf{r} - \mathbf{r}'|} d\mathbf{r}' \quad (1)$$

The vector potential A is decoupled from the electric field E which is calculated using equation (2) where $\nabla \cdot \mathbf{E}_s = 0$ (solenoidal) and $\nabla \times \mathbf{E}_i = 0$ (irrotational).

$$\mathbf{E} = -j\omega\mathbf{A} + \nabla\varphi = \mathbf{E}_s + \mathbf{E}_i \quad (2)$$

The magneto-quasi-static calculation is described by equation (3).

$$\nabla \cdot \sigma \nabla \varphi = j\omega \nabla \cdot (\sigma \mathbf{A}_0) \quad (3)$$

Fig. 22 (a), (b), (c) and (d) show the difference in electric and magnetic fields generated in the head for different vertical positions of the large coil. When comparing Fig. 22(b) and Fig. 22(d), it shows that the electric field in Fig. 22(b) is higher than that in Fig. 22(d).

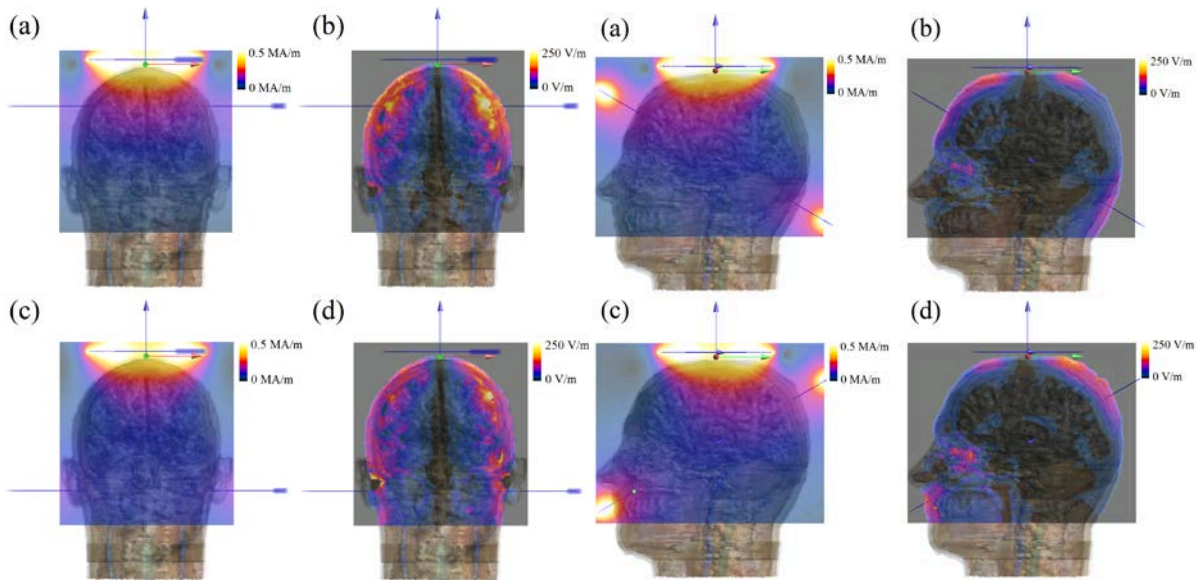


Fig. 22 Magnetic field (a and c) and electric field (b and d) generated in the anatomically realistic human head model for different vertical positions of the large coil. In figures a and b, the distance between two coils is 5 cm. In figures c and d, the distance between two coils is 15 cm.

Fig. 23 Magnetic field (a and c) and electric field (b and d) generated in the anatomically realistic human head model for different rotational angles of the large coil. In figures a and b, the coil is rotated +30 degrees. In figures c and d, the coil is rotated -30 degrees.

However, the electric field in lower part of head model is higher in Fig .22(b) than in Fig .22(d), which is enhanced by the position of the large coil. These modeling results show the evidence that the larger coil enhances the electric and magnetic fields at the deeper regions of the brain by reducing the decay of field generated by the smaller circular coil which is fixed on the top of head. Thus, different positions of larger coil enables stimulation

of different deeper regions of the human brain and helps clinicians to vary the site of stimulation according to the disorder that is being treated.

Fig. 23 shows the induced electric field in the anatomical heterogeneous head model with the rotational movement of the larger coil. According to Fig. 23 (b) and (d), the position of the peak value of the electric field was different according to different positions of the larger coil and the peak value of electric field was approximately 250 V/m which is larger than the threshold electric field of 150 V/m reported by March *et al.* [5] and 120 V/m by Rosanova *et al.* [6]. Therefore, rotation of the larger coil also reduces the decay of electric and magnetic field generated by the small circular coil similar to vertical movement.

References

- [1] L. J. Crowther, P. Marketos, P. I. Williams, Y. Melikhov, D. C. Jiles, and J. H. Starzewski, "Transcranial magnetic stimulation: Improved coil design for deep brain investigation," *J. Appl. Phys.*, vol. 109, no. 7, pp. 2009–2012, 2011.
- [2] A. Christ, W. Kainz, E. G. Hahn, K. Honegger, M. Zefferer, E. Neufeld, W. Rascher, R. Janka, W. Bautz, J. Chen, B. Kiefer, P. Schmitt, H.-P. Hollenbach, J. Shen, M. Oberle, D. Szczerba, A. Kam, J. W. Guag, and N. Kuster, "The Virtual Family--development of surface-based anatomical models of two adults and two children for dosimetric simulations.," *Phys. Med. Biol.*, vol. 55, no. 2, pp. N23–38, Jan. 2010.
- [3] Hasgall PA, Di Gennaro F, Baumgartner C, Neufeld E, Gosselin MC, Payne D, Klingensböck A, Kuster N, "IT"IS Database for thermal and electromagnetic parameters of biological tissues," Version 2.6, January 13th, 2015. www.itis.ethz.ch/database
- [4] P. I. Williams, P. Marketos, L. J. Crowther, and D. C. Jiles, "New Designs for Deep Brain Transcranial Magnetic Stimulation," *IEEE Trans. Magn.*, vol. 48, no. 3, pp. 1171–1178, Mar. 2012.
- [5] S. March, S. Stark, M. Hadimani, D. Stiner, M. Senter, K. Spoth, L. Crowther, and D. Jiles, "Thermal and Mechanical Analysis of Novel Transcranial Magnetic Stimulation Coil for Mice," *IEEE Trans. Magn.*, vol. PP, no. 99, pp. 1–1, 2014.
- [6] M. Rosanova, A. Casali, V. Bellina, F. Resta, M. Mariotti, and M. Massimini, "Natural frequencies of human corticothalamic circuits.," *J. Neurosci.*, vol. 29, no. 24, pp. 7679–85, Jun. 2009.

**APPENDIX B. LIST OF PUBLICATIONS AND REPRINTS OF
PUBLICATIONS DERIVED FROM THE WORK PERFORMED FOR THIS
THESIS**

Archived Journal Publications:

1. **Y. Meng**, R. L. Hadimani, L. J. Crowther, V. Anantharam, A. G. Kanthasamy, and D. C. Jiles, "Differential Effect of Magnetic Field Orientation on the Proliferation Rate of Dopaminergic Neurons during Transcranial Magnetic Stimulation, Submitted to *Neuroscience of Elsevier*
2. **Y. Meng**, R. L. Hadimani, L. J. Crowther, Z. Xu, J. Qu, and D. C. Jiles, "Deep brain transcranial magnetic stimulation using variable 'Halo coil' system," *J. Appl. Phys.*, vol. 117, no. 17, p. 17B305, 2015.

Peer Reviewed Conference Publications:

1. **Y. Meng**, J. Qu, Z. Xu, L. J. Crowther, R. L. Hadimani, and D. C. Jiles, "Development of Adjustable ' Halo Coil ' Configuration for Deep Brain Transcranial Magnetic Stimulation," 36th Annual International IEEE EMBS Conference, Chicago, IL, USA, August 26-30,2014
2. **Y. Meng**, R. L. Hadimani, V. Anantharam, A. G. Kanthasamy, and D. C. Jiles, "Differential Effect of Magnetic Field Orientation on the Growth Rate of Dopaminergic Neurons during Transcranial Magnetic Stimulation," 36th Annual International IEEE EMBS Conference, Chicago, IL, USA, August 26-30,2014
3. **Y. W. Meng**, J. K. Qu, R. L. Hadimani, L. J. Crowther and D. C. Jiles, "*Development of Variable "Halo Coil" Configuration for Deep Brain Transcranial Magnetic Stimulation*" Minnesota Neuromodulation Symposium, Minneapolis, USA, April 2014
4. **Y. Meng**, R.L. Hadimani, V. Anantharam, A.G. Kanthasamy, and D.C.Jiles. "Control of proliferation rate of N27 dopaminergic neurons using Transcranial Magnetic Stimulation orientation." *Bulletin of the American Physical Society* 60, (2015)

Deep brain transcranial magnetic stimulation using variable “Halo coil” system

Y. Meng, R. L. Hadimani,^{a)} L. J. Crowther, Z. Xu, J. Qu, and D. C. Jiles

Department of Electrical and Computer Engineering, Iowa State University, Ames, Iowa 50011, USA

(Presented 7 November 2014; received 22 September 2014; accepted 28 October 2014; published online 4 March 2015)

Transcranial Magnetic Stimulation has the potential to treat various neurological disorders non-invasively and safely. The “Halo coil” configuration can stimulate deeper regions of the brain with lower surface to deep-brain field ratio compared to other coil configurations. The existing “Halo coil” configuration is fixed and is limited in varying the site of stimulation in the brain. We have developed a new system based on the current “Halo coil” design along with a graphical user interface system that enables the larger coil to rotate along the transverse plane. The new system can also enable vertical movement of larger coil. Thus, this adjustable “Halo coil” configuration can stimulate different regions of the brain by adjusting the position and orientation of the larger coil on the head. We have calculated magnetic and electric fields inside a MRI-derived heterogeneous head model for various positions and orientations of the coil. We have also investigated the mechanical and thermal stability of the adjustable “Halo coil” configuration for various positions and orientations of the coil to ensure safe operation of the system. © 2015 AIP Publishing LLC.

[<http://dx.doi.org/10.1063/1.4913937>]

INTRODUCTION

Transcranial magnetic stimulation (TMS) is a painless and non-invasive neuromodulation technique based on the principles of magnetic induction.^{1,2} TMS has been used to study brain function and is being investigated as a possible treatment for numerous brain disorders.⁴ The technique already shows good efficacy for the treatment of major depressive disorder.³ We have previously reported a “Halo coil” configuration which can stimulate deeper regions of the human brain, but the configuration was fixed so that only a single site in the brain has a lower surface to deep-brain field ratio compared to other coil configurations.⁵ Now, we have built a variable “Halo coil” configuration with a circular coil fixed on top of the head and with vertical and rotational movement of the larger coil to selectively stimulate different regions of the brain. During the stimulation, we used two stimulators to send AC current signals to two coils. One stimulator sends an AC current with a frequency of 2.5 kHz and an amplitude of 2500 A to the circular coil. The other stimulator sends AC current with a frequency of 2.5 kHz and an amplitude of 5000 A to the larger coil. We have also conducted thermal and mechanical analysis of the system to ensure its feasibility and stability. A graphical user interface (GUI) system has been built that accurately controls the movement and rotation of the larger coil using an Arduino microcontroller.

MODELING OF ELECTRIC AND MAGNETIC FIELD

We have used SEMCAD X (SPEAG, Swiss) finite element software to calculate the electric and magnetic fields generated by the fixed circular coil positioned at the vertex of the head with different orientations of the larger coil. An

AC current with a frequency of 2.5 kHz and an amplitude of 2500 A was applied to the circular coil which is comparable to the pulse signal generated by a biphasic commercial TMS stimulator with 50% power intensity, and a current signal of the same frequency but with an amplitude of 5000 A was applied to the large coil.⁵ We have used an anatomically realistic human head model with different electrical properties assigned to each tissue of the brain.⁶ These parameters are shown in Table I.⁷

The calculation of magnetic field was based on the Biot-Savart law as shown in the following equation:⁸

$$\mathbf{A}_0(\mathbf{r}) = \frac{\mu_0}{4\pi} \int_{\Omega} \frac{\mathbf{J}_0(\mathbf{r}')}{|\mathbf{r} - \mathbf{r}'|} d\mathbf{r}'. \quad (1)$$

The vector potential \mathbf{A} is decoupled from the electric field \mathbf{E} which is calculated using Eq. (2) where $\nabla \cdot \mathbf{E}_s = 0$ (solenoidal) and $\nabla \times \mathbf{E}_i = 0$ (irrotational)

$$\mathbf{E} = -j\omega\mathbf{A} + \nabla\varphi = \mathbf{E}_s + \mathbf{E}_i. \quad (2)$$

The magneto-quasi-static calculation is described by the following equation:

$$\nabla \cdot \sigma \nabla \varphi = j\omega \nabla \cdot (\sigma \mathbf{A}_0). \quad (3)$$

TABLE I. Values of dielectric properties at 2.5 kHz.

Tissue	ϵ_r (relative permittivity)	σ (Electric Conductivity) [S/m]
Brain (grey matter)	7.81×10^4	1.04×10^{-1}
Brain (white matter)	3.43×10^4	6.45×10^{-2}
Cerebellum	7.84×10^4	1.24×10^{-1}
Cerebrospinal fluid	1.09×10^2	2.00
Skin	1.14×10^3	2.00×10^{-4}
Skull	1.44×10^3	2.03×10^{-4}

^{a)}Author to whom correspondence should be addressed. Electronic mail: hadimani@iastate.edu.

Figs. 1(a)–1(d) show the difference in electric and magnetic fields generated in the head for different vertical positions of the large coil. When comparing Figs. 1(b) and 1(d), it shows that the electric field in Fig. 1(b) is higher than that in Fig. 1(d). However, the electric field in lower part of head model is higher in Fig. 1(b) than in Fig. 1(d), which is enhanced by the position of the large coil. These modeling results show the evidence that the larger coil enhances the electric and magnetic fields at the deeper regions of the brain by reducing the decay of field generated by the smaller circular coil which is fixed on the top of head. Thus, different positions of larger coil enable stimulation of different deeper regions of the human brain and helps clinicians to vary the site of stimulation according to the disorder that is being treated.

Fig. 2 shows the induced electric field in the anatomical heterogeneous head model with the rotational movement of the larger coil. According to Figs. 2(b) and 2(d), the position of the peak value of the electric field was different according to different positions of the larger coil and the peak value of electric field was approximately 250 V/m which is larger than the threshold electric field of 150 V/m, reported by March *et al.*⁹ and 120 V/m by Rosanova *et al.*¹⁰ Therefore, rotation of the larger coil also reduces the decay of electric and magnetic field generated by the small circular coil similar to vertical movement.

MAGNETIC (LORENTZ) FORCE RESPONSE

COMSOL Multiphysics (Los Angeles, CA, USA) was used for magnetic force analysis. A 5000 A DC current was assigned in both coils to evaluate the maximum forces induced on the variable “Halo coil” system. Any forces experienced by the coils will be transferred to the insulation

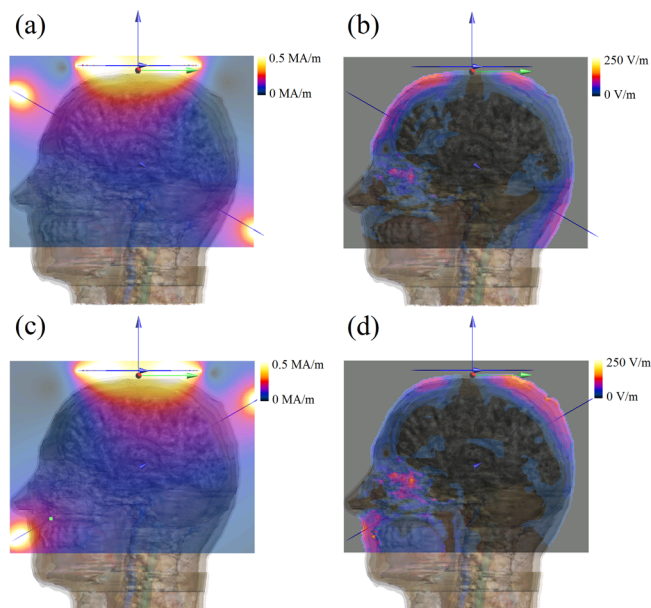


FIG. 2. Magnetic field ((a) and (c)) and electric field ((b) and (d)) generated in the anatomically realistic human head model for different rotational angles of the large coil. In figures (a) and (b), the coil is rotated $+30^\circ$. In figures (c) and (d), the coil is rotated -30° .

and thus the yield strength of insulation should be higher than the Lorentz forces exerted by the magnetic fields generated by the coils. The yield strength of copper is 70 MPa (Ref. 11) and the ultimate tensile strength of the insulation, Nylon is 125 MPa.¹² The Lorentz force density in the coil can be calculated by Eq. (4), where J (A/m) is the current density and B (T) is the magnetic flux density. In this study, we used 3D models where J (A/m³) is the current density and $i = x, y, z$

$$f_i = J \times B. \quad (4)$$

The calculated Lorentz force density f (N/m³) is shown in Fig. 3 for two extreme conditions for our system. The larger coil is rotated $+30^\circ$ and the distance between the centers of two coils is 5 cm and 15 cm. Fig. 3(a) is the top view and Fig. 3(b) is the side view for a distance of 5 cm between the coils. In Figs. 3(c) and 3(d), the distance between the centers of two coils is 15 cm, i.e., Fig. 3(c) is the top view and Fig. 3(d) is the side view.

The arrows in the picture show the direction of Lorentz forces and their lengths indicate the magnitude of that force density. In the side view, the majority of Lorentz force density was parallel to the direction of vertical movement of the large coil. The maximum Lorentz force was 335.01 MN/m³. The equivalent stress on the larger coil was 3.35 MPa. The coils are made of copper with a yield strength of 70 MPa and covered with Nylon, which has a yield/ultimate tensile strength of 125 MPa. Thus, the stress due to the Lorentz forces in the larger coil was significantly smaller than the yield strength of copper and Nylon. The system is therefore be mechanically stable and can withstand the expected Lorentz forces. However, the cyclic loading conditions, which can occur in repetitive TMS, have not been analyzed.

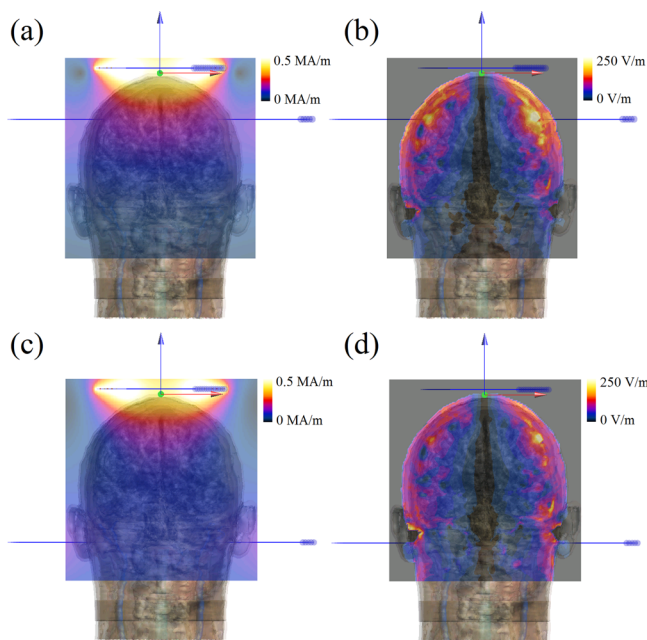


FIG. 1. Magnetic field ((a) and (c)) and electric field ((b) and (d)) generated in the anatomically realistic human head model for different vertical positions of the large coil. In figures (a) and (b), the distance between two coils is 5 cm. In figures (c) and (d), the distance between two coils is 15 cm.

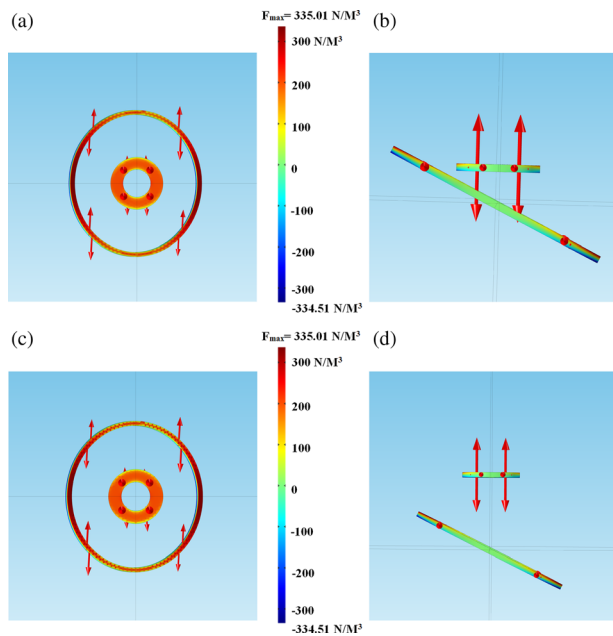


FIG. 3. The result of force analysis between the two coils with larger coil rotated at $+30^\circ$. In (a) and (b), the distance between the centers of two coils is 5 cm, where (a) is the top view and (b) is the side view. In (c) and (d), the distance between the centers of two coils is 15 cm, where (c) is the top view and (d) is the side view.

THERMAL ANALYSIS

The temperature in the coils was another important factor in the system because of the high amplitude of the current induced in the coil. This can generate a large amount of heat in the coil due to Joule's law ($Q = I^2 \cdot R \cdot t$). The limit of surface temperature for electrical medical equipment has been specified by General Standard IEC 60601-2-37, which is 50°C in air and 43°C at the surface of the body.¹³ Thus, the modeling of heat was focused on the duration of the stimulation when either of the coils reached 50°C . The incompressible Navier-Stokes heat equation from the COMSOL Heat Transfer module was used to model the thermal changes in the coil system under TMS therapy conditions, as shown in the following equation:

$$\rho C_p \frac{\partial T}{\partial t} + C_p u \cdot \nabla T = \nabla \cdot (k \nabla T) + Q, \quad (5)$$

where ρ is the fluid density, C_p is the fluid heat capacity, T is the temperature, u is the velocity field of the fluid, k is the thermal diffusivity of the material, and Q is external source heating.¹⁴ According to the modeling results shown in Fig. 4, after stimulation for 231 s, the small circular coil, which is placed on the top on patient's head, reached 50.04°C . Additionally, the vertical position and the rotational movement of the larger coil did not have a significant effect on the heat generated in the two coils as all positions and orientations demonstrated similar results of approximately 50°C in the smaller coil after 231 s of stimulation.

GUI SYSTEM

A GUI was developed in Java to control the movement and rotation of the larger coil with a computer via an

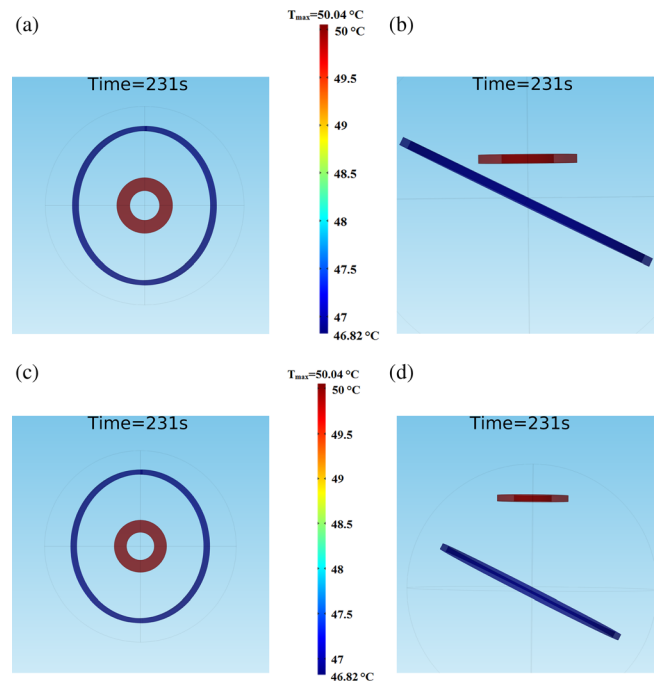


FIG. 4. The result of thermal analysis of two coils with larger coil rotated at $+30^\circ$. In (a) and (b), the distance between the centers of two coils is 5 cm, where (a) is the top view and (b) is the side view. In (c) and (d), the distance between the centers of two coils is 15 cm, where (c) is the top view and (d) is the side view.

Arduino microcontroller, as shown in Fig. 5. The left portion of the interface is the control panel, which has two buttons to control the vertical movement of large coil by a linear actuator. The range of vertical movement is -5 cm to $+5$ cm compared to its origin with a step size of 1 cm. It also has two buttons to control the rotation by a servo motor. The range of rotation is -30° to $+30^\circ$ compared to its origin with a step size of 5° . The right portion of the interface shows the modeling results of electric and magnetic field for the selected position of the large coil. These images will show the distribution of magnetic and electric field, which will indicate the site of stimulation with a field larger than the threshold or peak field for the selected position of the large coil.

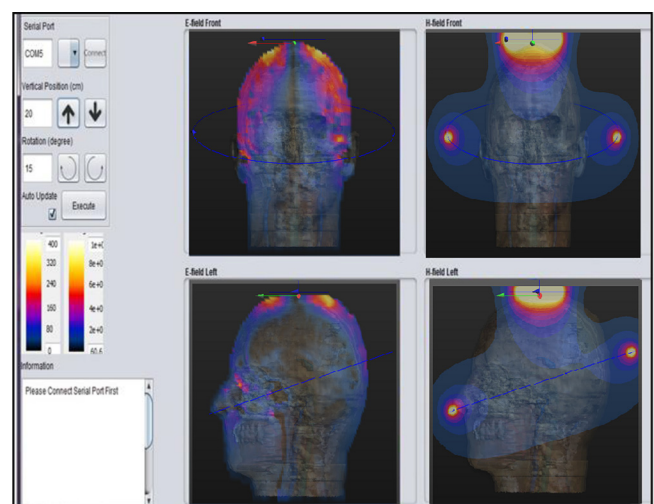


FIG. 5. The graphic user interface (GUI).

CONCLUSION

TMS is a novel non-invasive and safe treatment for various neurological disorders. In our present work, we have designed and developed a variable “Halo coil” system that can achieve deep brain stimulation at specific treatment areas with the vertical and rotational movement of the larger coil in the “Halo coil” system. We have also developed a GUI system to control the movement precisely via a computer. The modeling results of magnetic and electric field confirm that our design can stimulate different parts of human brain. The modeling result of Lorentz forces show that the magnetic forces in coils do not exceed the yield strengths of the coil material and casing in the system. The modeling results of Joule heating showed that the treatment time of 231 s will heat the coil to a temperature of 50.04 °C. Thus, for longer treatment times, an active cooling system using external air or water circulation should be considered.

ACKNOWLEDGMENTS

This work was supported by the Carver Charitable Trust and the Barbara and James Palmer Endowment at the Department of Electrical and Computer Engineering, Iowa State University.

- ¹A. T. Barker, R. Jalinous, and I. L. Freeston, *Lancet* **325**, 1106 (1985).
- ²P. J. Basser and B. J. Roth, *Med. Biol. Eng. Comput.* **29**, 261 (1991).
- ³S. Rossi, M. Hallett, P. M. Rossini, and A. Pascual-Leone, *Clin. Neurophysiol.* **120**, 2008 (2009).
- ⁴M. S. George, S. H. Lisanby, D. Avery, W. M. McDonald, V. Durkalski, M. Pavlicova, B. Anderson, Z. Nahas, P. Bulow, P. Zarkowski, P. E. Holtzheimer, T. Schwartz, and H. A. Sackeim, *Arch. Gen. Psychiatry* **67**, 507 (2010).
- ⁵L. J. Crowther, P. Marketos, P. I. Williams, Y. Melikhov, D. C. Jiles, and J. H. Starzewski, *J. Appl. Phys.* **109**, 07B314 (2011).
- ⁶A. Christ, W. Kainz, E. G. Hahn, K. Honegger, M. Zefferer, E. Neufeld, W. Rascher, R. Janka, W. Bautz, J. Chen, B. Kiefer, P. Schmitt, H.-P. Hollenbach, J. Shen, M. Oberle, D. Szczerba, A. Kam, J. W. Guag, and N. Kuster, *Phys. Med. Biol.* **55**, N23 (2010).
- ⁷P. A. Hasgall, F. Di Gennaro, C. Baumgartner, E. Neufeld, M. C. Gosselin, D. Payne, A. Klingenböck, and N. Kuster, “IT’IS Database for thermal and electromagnetic parameters of biological tissues,” Version 2.5, August 1st, 2014, available at www.itis.ethz.ch/database.
- ⁸L. J. Crowther, K. Porzig, R. L. Hadimani, H. Brauer, and D. C. Jiles, *IEEE Trans. Magn.* **48**, 4058 (2012).
- ⁹S. D. March, S. McAtee, M. Senter, K. Spoth, D. R. Stiner, L. J. Crowther, R. L. Hadimani, and D. C. Jiles, “Focused and deep brain magnetic stimulation using new coil design in mice,” *2013 6th Int. IEEE/EMBS Conf. Neural Eng.*, Nov. 2013, pp. 125–128.
- ¹⁰M. Rosanova, A. Casali, V. Bellina, F. Resta, M. Mariotti, and M. Massimini, *J. Neurosci.* **29**, 7679 (2009).
- ¹¹L. J. Crowther, K. Porzig, R. L. Hadimani, H. Brauer, and D. C. Jiles, *IEEE Trans. Magn.* **49**, 3426 (2013).
- ¹²H. Mahfuz, A. Adnan, V. K. Rangari, M. M. Hasan, S. Jeelani, W. J. Wright, and S. J. DeTeresa, *Appl. Phys. Lett.* **88**, 083119 (2006).
- ¹³IEC IS 60601: Medical Electrical Equipment—Part 2-37, 2005.
- ¹⁴S. March, S. Stark, R. L. Hadimani, D. Stiner, M. Senter, K. Spoth, L. Crowther, and D. Jiles, *IEEE Trans. Magn.* **50**, 5100805 (2014).

Differential Effect of Magnetic Field Orientation on the Proliferation Rate of Dopaminergic Neurons during Transcranial Magnetic Stimulation

Y. Meng¹, R. L. Hadimani¹, L. J. Crowther¹, V. Anantharam², Gary Zenitsky², A. Kanthasamy² and D. C. Jiles¹

¹*Dept. of Electrical and Computer Engineering, Iowa State University, Ames, IA 50011 USA*

²*Department of Biomedical Sciences, Iowa State University, Ames, IA 50011, USA*

Abstract--Transcranial magnetic stimulation (TMS) has been used to investigate possible treatments for a variety of neurological disorders. But the effect that magnetic fields have on neurons has not been well documented in the literature. Using a monophasic stimulator, we investigated the effect of different orientation of magnetic field generated by TMS coils on the proliferation rate of N27 neuronal cells cultured in flasks and multi-well plates. Exposing horizontally adherent N27 cells to a magnetic field pointing upward through the neuronal proliferation layer increased the proliferation of cells compared with the control group. On the other hand, proliferation rate decreased in cells exposed to a magnetic field pointing downward through the neuronal growth layer compared with the control group. The results were consistent across different methods of measuring proliferation and cell counting procedures. We confirmed results obtained from the Trypan-blue and automatic cell counting methods with those from the CyQuant and MTS cell viability assays. Our findings could have important implications for the preclinical development of TMS treatments of neurological disorders and represents a new method to control the proliferation rate of neuronal cells.

Key words: TMS; dopaminergic neurons; proliferation rate; orientation of magnetic field

INTRODUCTION

Transcranial Magnetic Stimulation is a non-invasive neuromodulation technique that uses time varying short pulses of magnetic field to induce an electric field in the conductive tissues of the brain thus, modulating the synaptic transmission of neurons. This neuromodulation technique can be used to excite or inhibit the firing rate of neurons which can then be used for treatment of various neurological disorders such as major depressive disorder, Parkinson's disease, Post-traumatic stress disorder and migraine (Barker

et al.,1985; George et al.,2010; Vonloh et al.,2013; Rosenberg 2002; Dodick et al.,2010). Since the US Food and Drug Administration (FDA) approved TMS as a treatment for depression in 2008, there has been less focus on *in vitro* and animal studies in the literature compared to *in vivo* studies in humans (Meng et al.,2015; Crowther et al.,2013; Wassermann and Zimmermann, 2012; March et al.,2014). The effects of TMS on individual neurons need to be thoroughly understood to fully utilize TMS as a neuromodulation tool for treating neurological disorders especially those originating from subcortical regions of the brain.

Few articles have reported the effect of time-varying magnetic fields, similar to those generated by TMS, on the proliferation rates of neurons. (Bonmassar et al.,2009) designed micro TMS coils and showed that the direction of magnetic field affects the firing frequency of neurons, but the authors did not report the effect of magnetic field on the proliferation rate. Meanwhile, some articles have reported the effect of static magnetic field on cell's proliferation rate (Miyakoshi 2009). Authors have used static magnetic fields from 1 to 10 tesla and did not find any significant effect on cell proliferation or on genetic toxicity, regardless of the length of treatment. However, there was a small effect on intracellular Ca^{2+} ion control. Some articles have reported beneficial effects of DC electric field (EF) on neural proliferation and differentiation. The EF gradient affects morphology and phenotype of adult neural stem/progenitor cells (NPCs), which shows the potential of utilizing EF to control migration, differentiation and alignment of stem cells transplanted to treat nervous system disorders (Ariza et al.,2010). Extremely low-frequency electromagnetic fields (ELF-EMFs) have been used therapeutically to drive cardiac-specific differentiation in adult human cardiac progenitor cells without any pharmacological or genetic manipulation of cells (Gaetani et al.,2009). As far as we know, no one has published on the effect of TMS magnetic field on the proliferation rate of neurons or on the morphology of cells.

In this paper, we have presented the effect of magnetic field generated by TMS coils on the proliferation of N27 dopaminergic neurons. We have used different cell proliferation and cell counting procedures to confirm that directing a magnetic field downward or upward through the horizontal proliferation plane of adherent cell cultures decreased or increased cell proliferation rates, respectively. It is

important to note that the direction of the induced electric current from the time varying TMS fields will be in clockwise or counterclockwise loops when the magnetic field is in up or down direction of the cell culture as shown in Fig. 4. This experimental set up is similar to the TMS treatment on human brain where the induced electric field from the TMS coils will be in clockwise or counterclockwise loops in the cortex.

EXPERIMENTAL PROCEDURES

A. Magnetic Field Generated by TMS coils

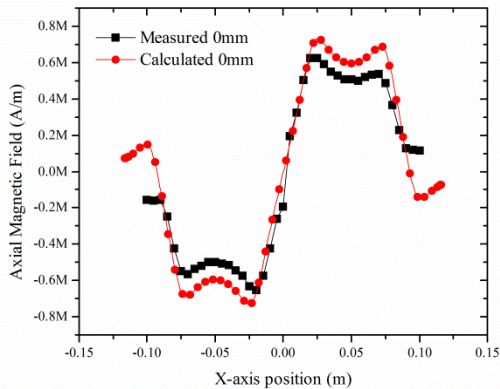


Fig.1 The axial component of magnetic field intensity along the diameter of a Magtism® Standard 70 mm double coil at coil surface. The red line is simulation result from SEMCAD X and the black line is measured result using gauss meter. The intensity of Magstim Rapid² stimulator was 100%.

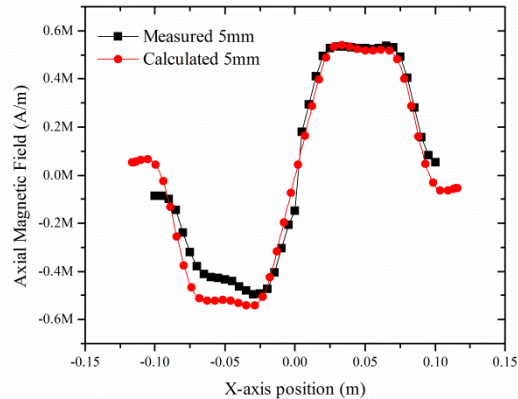


Fig. 2 The axial component of magnetic field intensity along the diameter of a Magtism® Standard 70 mm double coil at height of 5mm above coil surface. The red line is simulation result from SEMCAD X and the black line is measured result using gauss meter. The intensity of Magstim Rapid² stimulator was 100%.

A Magstim Standard 70 mm double coil was used for treating N27 neurons. Magnetic field was measured on the surface of the coil using a gaussmeter and a hall probe. The field was also calculated using finite element electromagnetic modeling software, SEMCAD X. The measured and calculated axial components of the magnetic field intensities are shown in Fig.1 and Fig.2. Magnetic field is negative in the negative x-axis and positive in the positive x-axis which is shown Fig. 2. It also shows magnetic field values at 5mm above the coil surface where dopaminergic neurons are placed during TMS treatment after considering the thickness of flask and thermal insulation layer. According to these figures, the peak value of measured magnetic field intensity at 5mm above the coil surface is 0.55 MA/m which is reduced by approximately 0.1MA/m. Fig. 3 shows the top view of distribution of magnetic field intensity generated by double coil. Fig.4 shows the different orientations of magnetic field generated by the coil and directions of

current in each circle of the double coil. The red arrows on the left indicate the directions of supplied current (5000 A) in left circle as counterclockwise and clockwise in the right circle. The cross symbols indicate the magnetic flux pointing into the plane and the dot symbols indicate the magnetic flux pointing out of the plane.

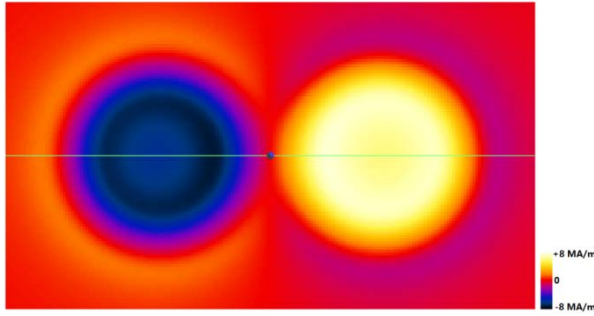


Fig. 3 Distribution of magnetic field intensity of double coil (2D top view).

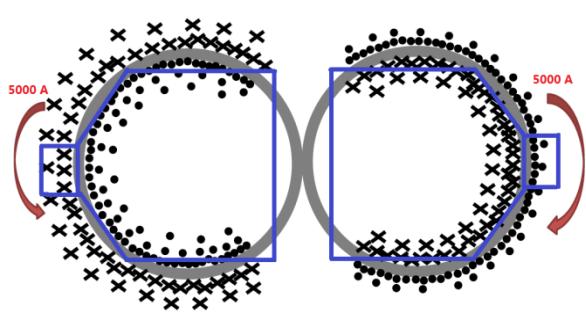


Fig. 4 Orientation of magnetic flux lines generated by double coil, cross representing upward and dot representing downward field. The red arrows show the direction of supplied current with a peak magnitude of 5000 A. The two blue polygons represent the two flasks.

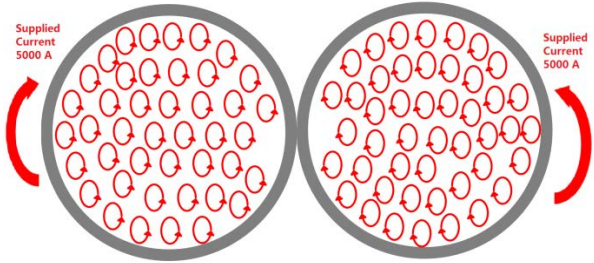


Fig. 5 Distribution of induced current on the coil plane at the first half of period of supplied current (2D top view).

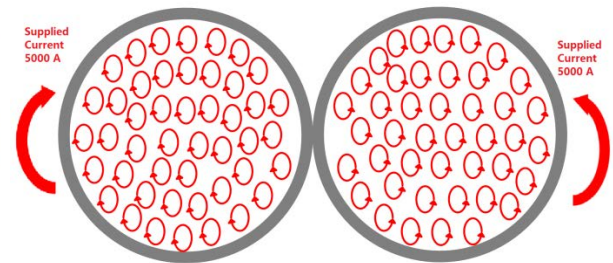


Fig. 6 Distribution of induced current on the coil plane at the second half of period of supplied current (2D top view).

According to Maxwell's equation, time-varying magnetic field will generate an electric field which induces eddy currents in the conducting neurons. The supplied current is a pulse wave which has a frequency of 2.5 kHz and magnitude of 5000 A, so its period is 0.4 ms. The stimulator sends only one pulse with a current amplitude of 5000 A in clockwise and counterclockwise directions in left and right circles of the coil respectively as shown in Fig. 4. Thus, the supplied current in each circular coil will generate a time varying magnetic field change from 0 to its peak value, during its first half period, which results in the corresponding induced eddy current in both areas shown in Fig. 5 and Fig. 6. According to

Lenz's law the induced current in the left circular coil was counterclockwise and it was clockwise in the right circular coil. Similarly, the value of the supplied current in both coils would change from its peak of 5000 A to 0 during the second half period. Thus, the induced eddy current on the left and right flasks was clockwise and counterclockwise, respectively. Therefore, the difference between the two flasks was the sequence of the direction of the eddy currents.

B. Cell Culture

Immortalized rat mesencephalic 1RB₃AN₂₇ cells (N27) were grown in RPMI-1640 medium supplemented with 10% fetal bovine serum, 1% L-glutamine, 50 units penicillin and 50 µg/ml streptomycin and maintained at 37°C with a humidified atmosphere containing 5% CO₂, as described previously (Anantharam et al.,2002; Prasad et al.,1998). On Day 0, an equal number of N27 cells were seeded into each T-75 flask or 96-well plate. Groups were distinguished by culture time with two control and two TMS groups per time point and four replicate samples (flask or plate) per group. Control 1 was always kept in the incubator and was named Incubator in Table I. Control 2 was kept in the biosafety cabinet during the TMS treatment and was named Environmental in Table I. Table I shows culture time points and counting time points for the different sample locations and magnetic field orientations ("Field up" and "Field down"), which were used in a Trypan blue cytotoxicity assay. Table II shows cell culture samples with their culture time points as well as counting time points used in a CyQuant cell proliferation assay. Table III shows culture samples with their culture and counting time points for an MTS cell viability assay and cell counting method. We performed a cell count for each sample of cells 24 hours after its TMS treatment to ensure that the cells had enough time to show any effects of TMS on their proliferation.

C. TMS experiment on dopaminergic neurons

We used a monophasic stimulator to treat N27 cell cultures. A set of 6 pulses with 4 seconds waiting time in between them was formed as one train and a waiting time of 10 seconds between each train was introduced, so the pulse repetition rate (TMS treatment frequency) we used is 0.25 Hz. This is a low frequency compared to usual clinical protocol frequency however, in order to obtain 100% power in the

coil and avoid rapid heating up of the coil we have used this low frequency. It is not possible to operate at higher frequencies at full power with the existing set-up. A total of 60 trains with 360 pulses were delivered per 30-minute TMS treatment. An air-cooled double coil was used which has opposite current directions in each coil, generating magnetic fields on top side of each coil with opposite directions. Using air-cooled coils allowed us to induce magnetic fields without raising the temperature of the T-75 flasks placed on them. All TMS treatments on N27 cells were performed in a sterile biosafety cabinet (Fig. 7). The flask set above the left coil was designated “Field up” and the flask set above the right coil was designated “Field down”, corresponding to the orientation of the magnetic fields.

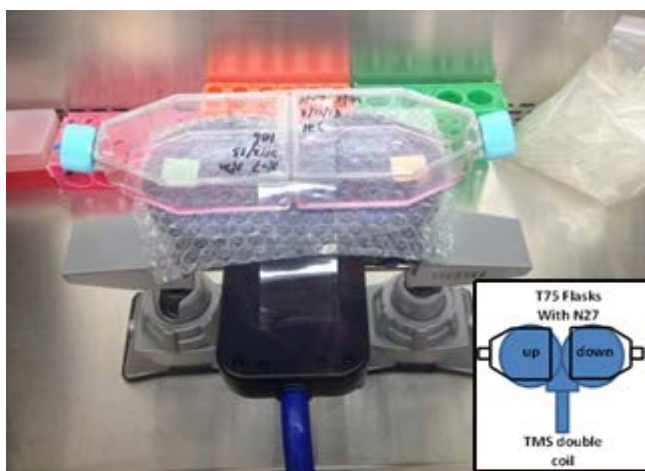


Fig. 7 Arrangement of the 30-minute TMS treatment delivered to two T-75 flasks. The directions of the two oppositely oriented magnetic fields were labeled on the double coil. Field orientation was upward on the left coil and downward on the right coil, as shown in the inset figure. We used two clamps to fix the coil in the cell culture cabinet and a layer of bubble wrap separated both flasks from the coils to maintain a thermal barrier.

D. Cytotoxicity assay

Cytotoxic cell death was measured as per Life Technologies’ Trypan blue exclusion cell counting method (Xu et al.,2008). Briefly, after treatment cells were harvested with trypsin-EDTA and resuspended in 1X PBS, we then took 10 μ l of cell suspension from one sample and added with 10 μ l of 0.4% trypan blue solution (Life Technologies) and triturated this mixture. Then, we put 10 μ l of the mixture into the cell counting slide and place the slide into the automatic cell counter to count the concentration of cells in each sample. Finally, we extrapolated the total number of cells in each sample by multiplying its volume and concentration (Xu et al.,2008). By using this method, we counted the

number of cells in each of the four replicate samples according to the counting time points shown in Table.

I. We studied the effect of TMS on 2 different initial cell densities, 1 million cells/flask and 0.5 million cells/flask (n=4).

Table I. Design of the TMS experiment with Trypan blue cell counting method for cell densities of 1 and 0.5 million cells /flask.

Culture Time point	Counting Time point	Sample Description			
		Incubator	Environmental	Field up	Field down
Day 0	Day 1	Incubator	Environmental	Field up	Field down
Day 0.5	Day 1.5	Incubator	Environmental	Field up	Field down
Day 1	Day 2	Incubator	Environmental	Field up	Field down
Day 1.5	Day 2.5	Incubator	Environmental	Field up	Field down
Day 2	Day 3	Incubator	Environmental	Field up	Field down

Table II. Design of the TMS experiment with CyQuant cell viability assay cell counting method for cell densities of 100k, 80k, 50k and 20k per well

Culture Time Point	Counting Time point	Sample Description		
		Environmental	Field up	Field down
Day 0	Day 1	Environmental	Field up	Field down
Day 1	Day 2	Environmental	Field up	Field down
Day 2	Day 3	Environmental	Field up	Field down

E. CyQuant cell proliferation assay

We used Life technologies' CyQuant cell viability assay to confirm our results from the Trypan blue cell counting procedures. On day 0, we seeded the N27 cells in 24-well plates (n=3) with the four rows per plate. In each plate, there were 4 rows and three columns. Row 1 to row 4 have different seeding densities; 20k, 50k, 80k, to 100k, respectively. Each row had three replicated samples in three columns to account for standard deviation. We had three groups with different culture times: Day 0, Day 1 and Day 2 (Table II). Briefly, after 24 hours post-treatment, we read the fluorescence with excitation maximum at 485 nm and the emission maximum at 530 nm using a Synergy 2 plate reader (BioTek) (Jones et al.,2001). We pooled the groups designated as Incubator and Environmental in Table I, because the difference between them was insignificant.

F. MTS cell viability assay cell counting method

Cell viability was measured using Promega's MTS assay to confirm the results from Trypan blue and CyQuant cell proliferation assays. Briefly, on day 0, we seeded the wells of 96-well plates with 15k for

one row and half with 20k for another row of N27 cells in 200 μ L of proliferation medium per well. Each row had 6 duplicated samples (n=6). The design of the experiment was according to Table III., TMS treatment was performed with “Field up” and “Field down” on 2 different well plates. After 24 hours post-treatment, 20 μ l MTS reagent (CellTiter 96® Aqueous One Solution Reagent) was added to each well and incubated at 37°C in a CO₂ incubator for 90 min and absorbance was read at 490 nm and 670 nm in a Spectramax plate reader (Molecular Devices). We subtracted the baseline via Abs₄₉₀-Abs₆₇₀ prior to data analysis (Mahon et al.,2000).

Table III. Design of the TMS experiment with MTS cell viability assay cell counting method for cell densities of 15k and 20k per well.

Culture Time Point	Counting Time point	Sample Description			
		Control	Environmental	Field up	Field down
Day 0	Day 1				

G. Statistical significance analysis

Statistical significance analysis was performed using Originlab 9.0 software (OriginLab Corporation, Northampton, MA, USA). Raw data analysis were analyzed using a two unpaired t-test. Statistically significant differences are indicated by asterisks as follows: *p<0.05, **p<0.01 and *p<0.001.

RESULTS

After TMS treatment of N27 cells, we counted the number of viable cells using the Trypan blue method for initial seeding densities of 1 million (Fig. 8) and 0.5 million (Fig. 9) cells per flask. The culture time and counting time points are indicated in Table I. The result showed that the proliferation rate increased after TMS stimulation with the magnetic field oriented upward through the horizontal plane of adherent cells, compared to incubator and environmental samples. The proliferation rate decreased when the field was oriented downward through the horizontal growth plane compared to incubator and environmental samples. Also, environmental samples exhibited slower proliferation compared to the incubator condition. For the lower seeding density (Fig.9), the difference of cell counting for each group became larger over time. The difference peaked on Day 3 when the number of cells in the “Field up” group was $23.57 \pm 3.21\%$

(mean \pm STD, *** p <0.001) higher than that in the Environmental group, while in the Field down group, it was $11.45 \pm 1.99\%$ (** p < 0.001) lower than in the Environmental group. Therefore, the total difference in cell's proliferation rate attributable to TMS field direction was +35.02 %.

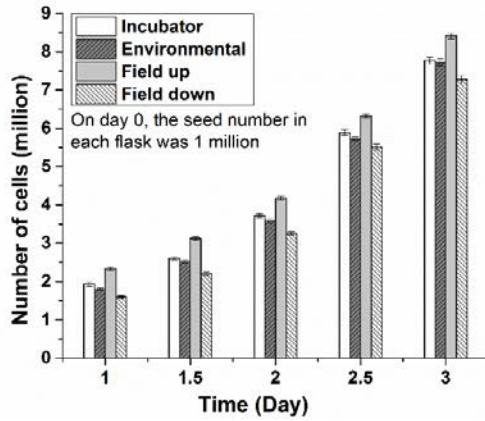


Fig. 8 Cell densities in the TMS experiment, derived using the Trypan blue cell counting method with an initial seeding density of 1 million cells/flask. Counting time is indicated in Table. I.

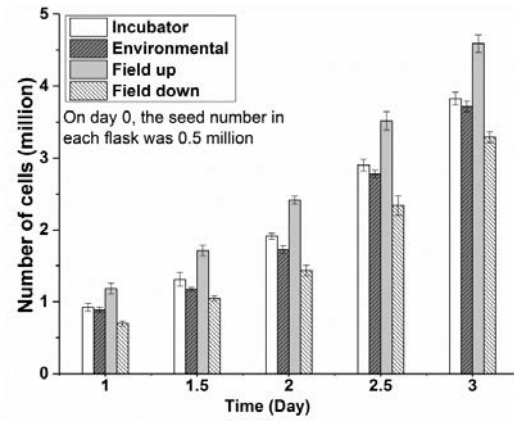


Fig. 9 Cell densities in the TMS experiment, derived using the Trypan blue cell counting method with initial seeding density of 0.5 million cells/flask. Counting time is indicated in Table. I.

To investigate the effect of different culture times on cell proliferation, we conducted another experiment expanding culture time up from 2 days to 2.5 days. The seeding density was 0.5 million/flask and the new culture time points were Day 0.5, Day 1, Day 1.5, Day 2 and Day 2.5. Cells were counted 24 h after each treatment, so the corresponding counting time points were Day 1.5, Day 2, Day 2.5, Day 3 and Day 3.5 respectively. The effect of TMS and its direction on the proliferation of cells over time (Fig. 10) was similar to the previous results for this seeding density (Fig. 9). On Day 3.5, the number of cells in the “Field up” group was $13.53 \pm 1.36\%$ (** p <0.001) higher than in the Environmental group, whereas the number of cells in the “Field down” group was $12.61 \pm 1.76\%$ (** p <0.001) lower than in the Environmental group. Therefore, the total difference in cell's proliferation rate attributable to TMS field direction was +26.14 %.

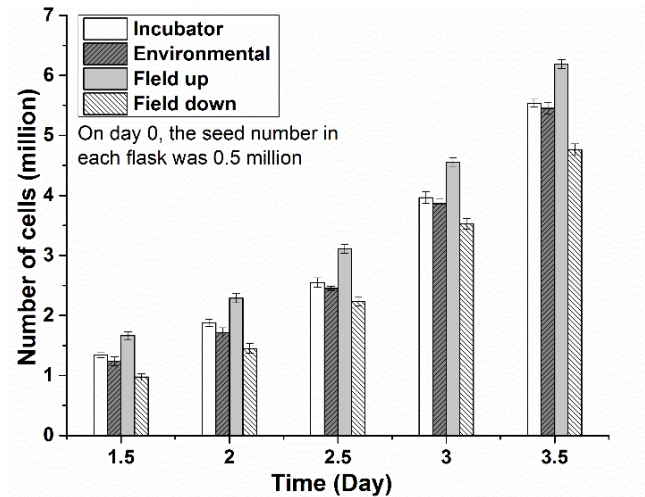


Fig. 10. Cell densities in the TMS experiment, derived using the Trypan blue cell counting method for an initial seeding density of 0.5 million cells/flask. Culture times were Day 0.5, Day 1, Day 1.5, Day 2 and Day 2.5. The corresponding Counting times were Day 1.5, Day 2, Day 2.5, Day 3 and Day 3.5, respectively.

We used the CyQuant cell viability assay to confirm the results obtained with the Trypan blue cell counting method. This time we eliminated group 1 (Incubator) and we set four seeding densities. The design of this experiment was based on Table II. The effect of TMS field direction on cell proliferation obtained via the CyQuant method (Fig 11-14) was similar to the effect measured using the Trypan blue cell counting method. However, Fig.8, which had the seeding density of 100k per well did not follow the trend similar to other seeding densities i.e. the difference in the proliferation rate was not pronounced. It may be due to the fact that a large number of cells grew in the limited space so the cells might have attained 100% confluency earlier than Day 3.

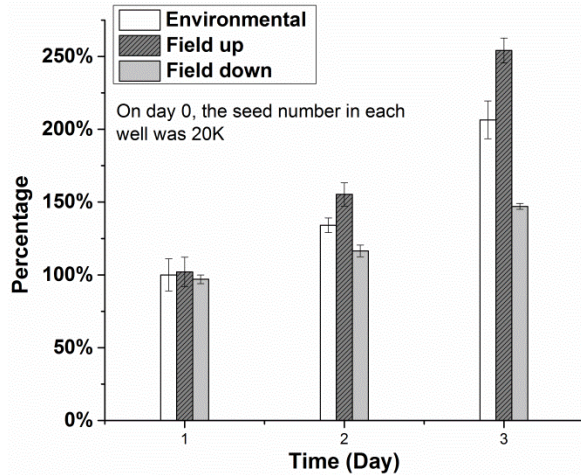


Fig. 11 Cell proliferation after TMS treatment of plates with an initial seeding density of 20k/well. We used the CyQuant cell viability assay to count cells. On day 3, the number of cells in the “Field up” group was $22.06 \pm 4.14\%$ (mean \pm STD as a percentage of the initial seeding density, * $p < 0.05$) higher than in the Environmental group, whereas cell numbers in the “Field down” group were $28.77 \pm 1.00\%$ (** $p < 0.01$) lower than in the Environmental group.

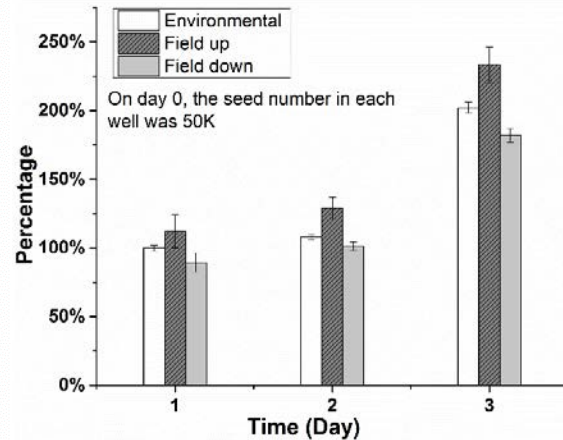


Fig.12 Cell proliferation after TMS treatment of plates with an initial seeding density of 50k/well. We used the CyQuant cell viability assay to count cells. On day 3, the number of cells in the “Field up” group was $15.49 \pm 7.26\%$ (mean \pm STD as a percentage of the initial seeding density, * $p < 0.05$) higher than in the Environmental group, whereas cell numbers in the “Field down” group were $9.94 \pm 2.47\%$ (* $p < 0.05$) lower than in the Environmental group.

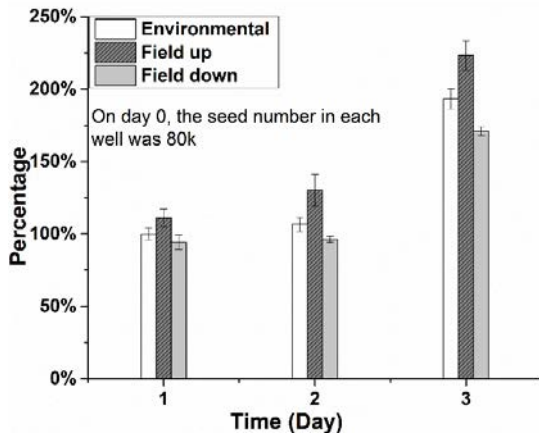


Fig. 13 Cell proliferation after TMS treatment of plates with an initial seeding density of 80k/well. We used the CyQuant cell viability assay to count cells. On day 3, the number of cells in the “Field up” group was $15.57 \pm 5.17\%$ (mean \pm STD as a percentage of the initial seeding density, * $p < 0.05$) higher than in the Environmental group, whereas cell numbers in the “Field down” group were $11.62 \pm 1.55\%$ (* $p < 0.05$) lower than in the Environmental group.

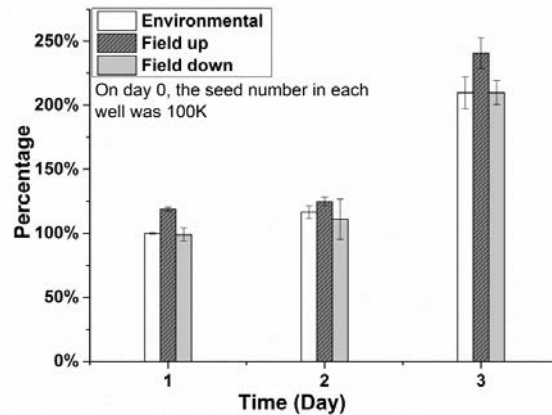


Fig. 14 Cell proliferation after TMS treatment of plates with an initial seeding density of 100k/well. We used the CyQuant cell viability assay to count cells. On day 3, the number of cells in the “Field up” group was $14.69 \pm 5.74\%$ (mean \pm STD as a percentage of the initial seeding density, $p > 0.05$) higher than in the Environmental group, whereas cell numbers in the “Field down” group were the same ($0 \pm 4.50\%$, $p > 0.05$) as those in the Environmental group.

A third cell counting method, the MTS cell viability assay, was performed to confirm the results obtained with the Trypan blue and CyQuant cell counting methods. With an initial seeding of 15k (Fig. 15), the number of cells in the “Field up” group was $19.88 \pm 4.56\%$ (** $p < 0.001$) higher than in the Environmental control group. Meanwhile, the number of cells in the “Field down” group was $8.88 \pm 1.39\%$ (** $p < 0.01$) lower than in the Environmental group. Next, using an initial seeding of 20k (Fig. 16), the number of cells in the “Field up” group was $19.60 \pm 4.57\%$ (** $p < 0.01$) higher than in the Environmental group, while the number of cells in the “Field down” group was $8.16 \pm 0.09\%$ (** $p < 0.01$) lower than in the Environmental group. Therefore, the total difference in cell’s proliferation rate attributable to TMS field direction was +27.76 %.

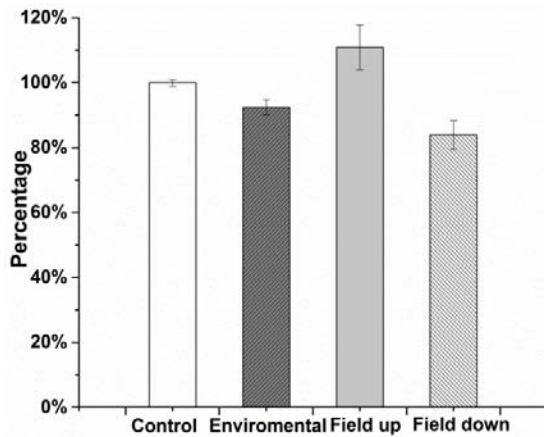


Fig. 15 Cell proliferation after TMS treatment of plates with an initial seeding density of 15k/well. We used the MTS cell viability assay to count cells, reported here as a percentage of control group1 (Incubator).

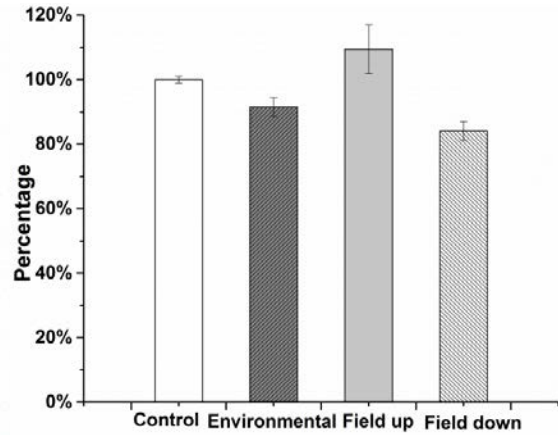


Fig. 16 Cell proliferation after TMS treatment of plates with an initial seeding density of 20k/well. We used the MTS cell viability assay to count cells, reported here as a percentage of control group1 (Incubator).

DISCUSSION

We investigated the effect of magnetic field orientation on the proliferation rate of N27 dopaminergic neuronal cells using three different cell counting methods to cross-validate the results. The MTS assay showed the highest difference in cell proliferation rate. It was also easy to replicate this counting procedure three times to obtain standard deviation. In the Trypan blue cell counting method, we used flasks to culture neuronal cells, which required more area to incubate replicate samples. Cell counting using the Trypan blue method was more time consuming because cell counting was performed one flask at a time, unlike the

MTS method where cell counting was performed in groups. There were three replicate samples for each group (n=3) for Trypan blue method and for MTS and CyQuant cell viability assay, n=6, which is adequate to show statistical significance. In the CyQuant cell viability cell counting method, it was easy to replicate samples and we were also able to count cells of all groups at once, but the differences among groups were slightly smaller than those from the MTS cell counting method. Thus, the MTS cell viability assay cell counting method is recommended for investigating the proliferation rate of N27 dopaminergic neuronal cells under TMS treatment.

According to the design of all these experiments, each group of N27 dopaminergic neuronal cells received a 30 minutes TMS treatment each day. After experimenting with a one-hour treatment, we found that increasing the treatment time did not make much difference on cell proliferation rate. We used 0.25 Hz as the actual frequency because the minimum discharging and recharging time for the capacitor is 4 seconds when we set intensity of the monophasic stimulator at 100%. This time can be reduced by setting a lower intensity. However, we have used 100% intensity in order to have significant effect on the growth/proliferation rate.. The temperature on the coil surfaces was measured by a thermal sensor which showed the temperature of the coil during stimulation. A temperature of 21.7 ± 0.1 °C was maintained in the flask and throughout the stimulation period. There was no obvious vibration of coils during the stimulation discerned by visually since the coil was fixed by two stages. Therefore, the difference in neural proliferation rate was due to the different orientation of magnetic field generated by double coil. Since during TMS was the corresponding electric field generated by time varying magnetic field can affect neurons firing rate (Bonmassar et al.,2012), different orientation of magnetic field will generate clockwise and counterclockwise electric fields and induced current in the brain. The difference in the sequence of clockwise and counterclockwise induced eddy current in the neurons is the reason for the different proliferation of neurons. Since, the interaction between magnetic field and neurons is not well established, further investigation of changes in neuron responses due to application of time varying magnetic fields such as TMS are warranted.

We plan to use different types of neuronal cells in future experiments to assess whether our results were cell-specific. We will also employ advanced imaging techniques to investigate any morphological changes in cells and cell components due to the effect of magnetic field orientation and stimulus parameters. Many factors potentially impact the proliferation of neuronal cells, such as BDNF, GDNF and NGF (Allen et al.,2013) so we will investigate the effects of TMS fields on these growth proteins.

CONCLUSIONS

The effect of magnetic field direction generated by TMS coils on the proliferation of N27 dopaminergic neuronal cells was investigated. Orienting the magnetic field upward through the horizontal plane of adherent cells increased their proliferation rate while orienting the magnetic field downward through the cell growth plane decreased their proliferation rate. The results obtained by the Trypan blue method of cell counting was verified by the CyQuant and MTS cell viability assay methods and all the results are statistically significant. The changes in cell proliferation rate due to magnetic field direction is an important step forward in understanding the effect of magnetic fields on neuronal cell biology. Our findings could have important implications for the preclinical development of TMS treatments of neurological disorders and represents a new method to control the proliferation rate of neuronal cells.

ACKNOWLEDGMENT

This work was supported by the Barbara and James Palmer Endowment and the Carver Charitable Trust at the Department of Electrical and Computer Engineering, Iowa State University.

REFERENCE

- Allen SJ, Watson JJ, Shoemark DK, Barua NU, Patel NK (2013) GDNF, NGF and BDNF as therapeutic options for neurodegeneration. *Pharmacol Ther* 138:155–175
- Anantharam V, Kitazawa M, Wagner J, Kaul S, Kanthasamy AG (2002) Caspase-3-dependent proteolytic cleavage of protein kinase Cdelta is essential for oxidative stress-mediated dopaminergic cell death after exposure to methylcyclopentadienyl manganese tricarbonyl. *J Neurosci* 22:1738–1751.

- Ariza CA, Fleury AT, Tormos CJ, Petruk V, Chawla S, Oh J, Sakaguchi DS, Mallapragada SK (2010) The influence of electric fields on hippocampal neural progenitor cells. *Stem Cell Rev* 6:585–600
- Barker AT, Jalinous R, Freeston IL (1985) Non-invasive magnetic stimulation of human motor cortex. *Lancet* 325:1106–1107
- Bonmassar G, Lee SW, Freeman DK, Polasek M, Fried SI, Gale JT (2012) Microscopic magnetic stimulation of neural tissue. *Nat Commun* 3:921
- Crowther LJ, Hadimani RM, Jiles DC (2013) A numerical dosimetry study for pediatric transcranial magnetic stimulation. In: 2013 6th International IEEE/EMBS Conference on Neural Engineering (NER), pp 239–242.
- Dodick DW, Schembri CT, Helmuth M, Aurora SK (2010) Transcranial magnetic stimulation for migraine: a safety review. *Headache* 50:1153–1163
- Gaetani R, Ledda M, Barile L, Chimenti I, De Carlo F, Forte E, Ionta V, Giuliani L, D’Emilia E, Frati G, Miraldi F, Pozzi D, Messina E, Grimaldi S, Giacomello A, Lisi A (2009) Differentiation of human adult cardiac stem cells exposed to extremely low-frequency electromagnetic fields. *Cardiovasc Res* 82:411–420
- George MS, Lisanby SH, Avery D, McDonald WM, Durkalski V, Pavlicova M, Anderson B, Nahas Z, Bulow P, Zarkowski P, Holtzheimer PE, Schwartz T, Sackeim HA (2010) Daily left prefrontal transcranial magnetic stimulation therapy for major depressive disorder: a sham-controlled randomized trial. *Arch Gen Psychiatry* 67:507–516
- Jones LJ, Gray M, Yue ST, Haugland RP, Singer VL (2001) Sensitive determination of cell number using the CyQUANT® cell proliferation assay. *J Immunol Methods* 254:85–98

- Mahon X, Deininger MWN, Schultheis B, Reiffers J, Goldman JM, Melo J V (2000) Selection and characterization of BCR-ABL positive cell lines with differential sensitivity to the tyrosine kinase inhibitor STI571 : diverse mechanisms of resistance *Franc.* 96:1070–1079.
- March S, Stark S, Hadimani RM, Stiner D, Senter M, Spoth K, Crowther L, Jiles D (2014) Thermal and Mechanical Analysis of Novel Transcranial Magnetic Stimulation Coil for Mice. *IEEE Trans Magn PP*:1–1
- Meng Y, Hadimani RM, Crowther LJ, Xu Z, Qu J, and Jiles DC (2015) Deep brain transcranial magnetic stimulation using variable ‘Halo coil’ system. *J. Appl. Phys* 117: 17, p. 17B305
- Miyakoshi J (2005) Effects of static magnetic fields at the cellular level. *Prog Biophys Mol Biol* 87:213–223
- Prasad KN, Clarkson ED, Rosa FG La, Edwards-prasad J, Freed CR (1998) MINIREVIEW Efficacy of Grafted Immortalized Dopamine Neurons in an Animal Model of Parkinsonism : A Review. 9:1–9.
- Rosenberg PB (2002) Repetitive Transcranial Magnetic Stimulation Treatment of Comorbid Posttraumatic Stress Disorder and Major Depression. *J Neuropsychiatr* 14:270–276
- Vonloh M, Chen R, Kluger B (2013) Safety of transcranial magnetic stimulation in Parkinson’s disease: a review of the literature. *Parkinsonism Relat Disord* 19:573–585
- Wassermann EM, Zimmermann T (2012) Transcranial magnetic brain stimulation: therapeutic promises and scientific gaps. *Pharmacol Ther* 133:98–107
- Xu Q, Kanthasamy AG, Reddy MB (2008) Neuroprotective effect of the natural iron chelator, phytic acid in a cell culture model of Parkinson’s disease. *Toxicology* 245:101–108